Electronic Supplementary Information

Computer-aided design of Pt/In_2O_3 single-atom catalysts for CO_2 hydrogenation to methanol

Yuchen Wang[a,b,c,†], Zixuan Zhou[a,b,†], Bin Qin[a,†], Qingyu Chang[a,†], Shanshan Dang[a], Yiqin Hu[d], Kun Li[c], Yuanjie Bao[a,b], Jianing Mao[b,e], Haiyan Yang[a], Yang Liu[c], Jiong Li[e], Shenggang Li[a,b,c,f*], David A. Dixon,[d*] Yuhan Sun[a,c,g], Peng Gao[a,b,f*]

[a] CAS Key Laboratory of Low-Carbon Conversion Science and Engineering, Shanghai Advanced Research Institute, Chinese Academy of Sciences, Shanghai 201210, China
[b] University of Chinese Academy of Sciences, Beijing 100049, China
[c] School of Physical Science and Technology, ShanghaiTech University, Shanghai 201210, China

[d] Department of Chemistry and Biochemistry, The University of Alabama, Shelby Hall, Box 870336, Tuscaloosa, Alabama 35487-0336, USA
[e] Shanghai Synchrotron Radiation Facility, Shanghai Advanced Research Institute, Chinese Academy of Sciences, Shanghai 201204, China
[f] *State Key Laboratory of Low Carbon Catalysis and Carbon Dioxide Utilization, Shanghai Advanced Research Institute, Chinese Academy of Sciences, Shanghai 201210, China*
[g] Shanxi Research Institute, Huairou Research Laboratory, Taiyuan 030032, China
[†] These authors contributed equally: Yuchen Wang, Zixuan Zhou, Qingyu Chang.

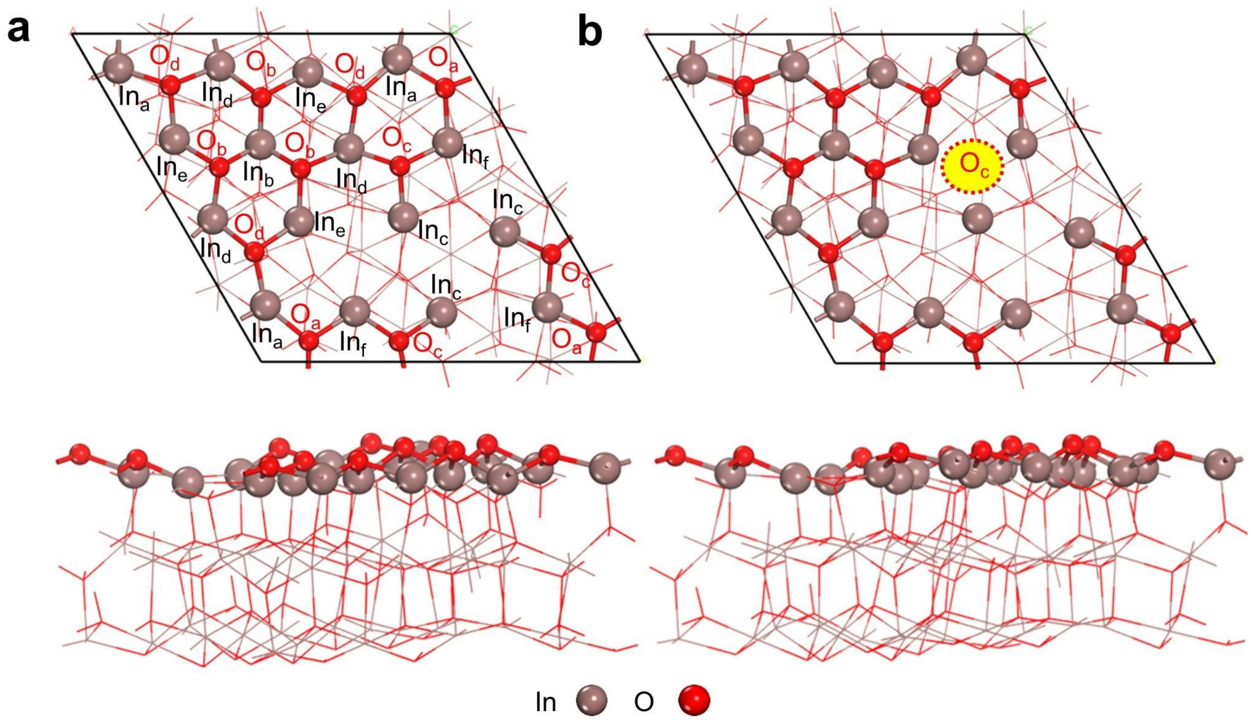

Figure S1. Structures of the pristine In_2O_3(111) surfaces. (**a**) Top and side views of the stoichiometric In_2O_3(111) surface. (**b**) Top and side views of the defective In_2O_3(111) surface with a V_O site located at the O_c site.

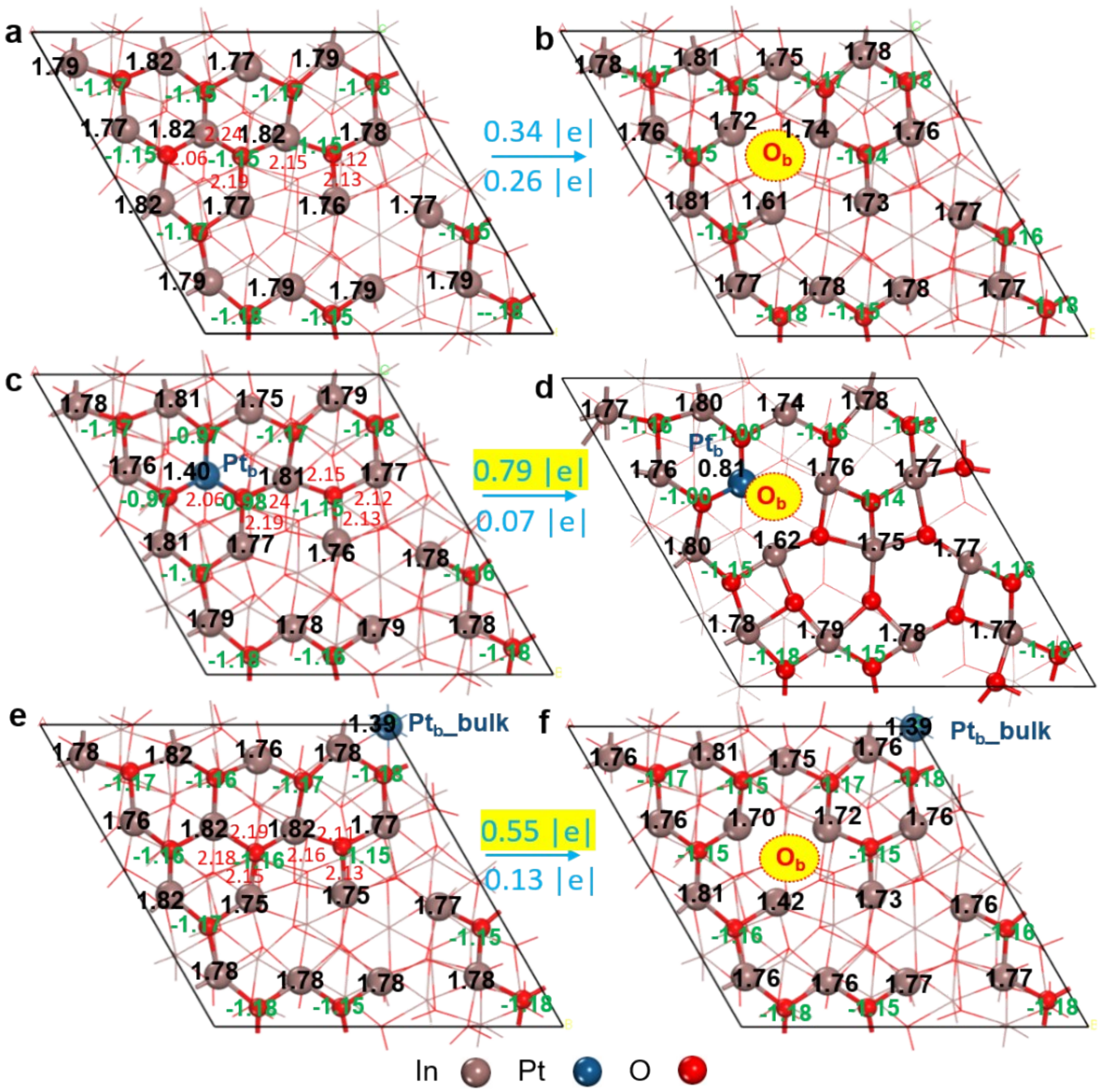

Figure S2. Calculated Bader charges of pristine In_2O_3(111) (**a**), surface-doped Pt/In_2O_3 (**c**) and bulk-doped Pt/In_2O_3 (**e**) and those structures with the O_{b_vac} site (**b**, **d**, **f**), where values in black are the positive charges of the surface metal sites (In/Pt), and those in green are the negative charges of the surface O sites (values in red are the metal-oxygen bond lengths in Å). The numbers above the blue arrows represent the total amount of charges transferred from the In_6, In_7, and In_{10} sites after V_O formation, whereas the numbers below the blue arrows represent those transferred from the In_7, In_8, and In_{11} sites after V_O formation.

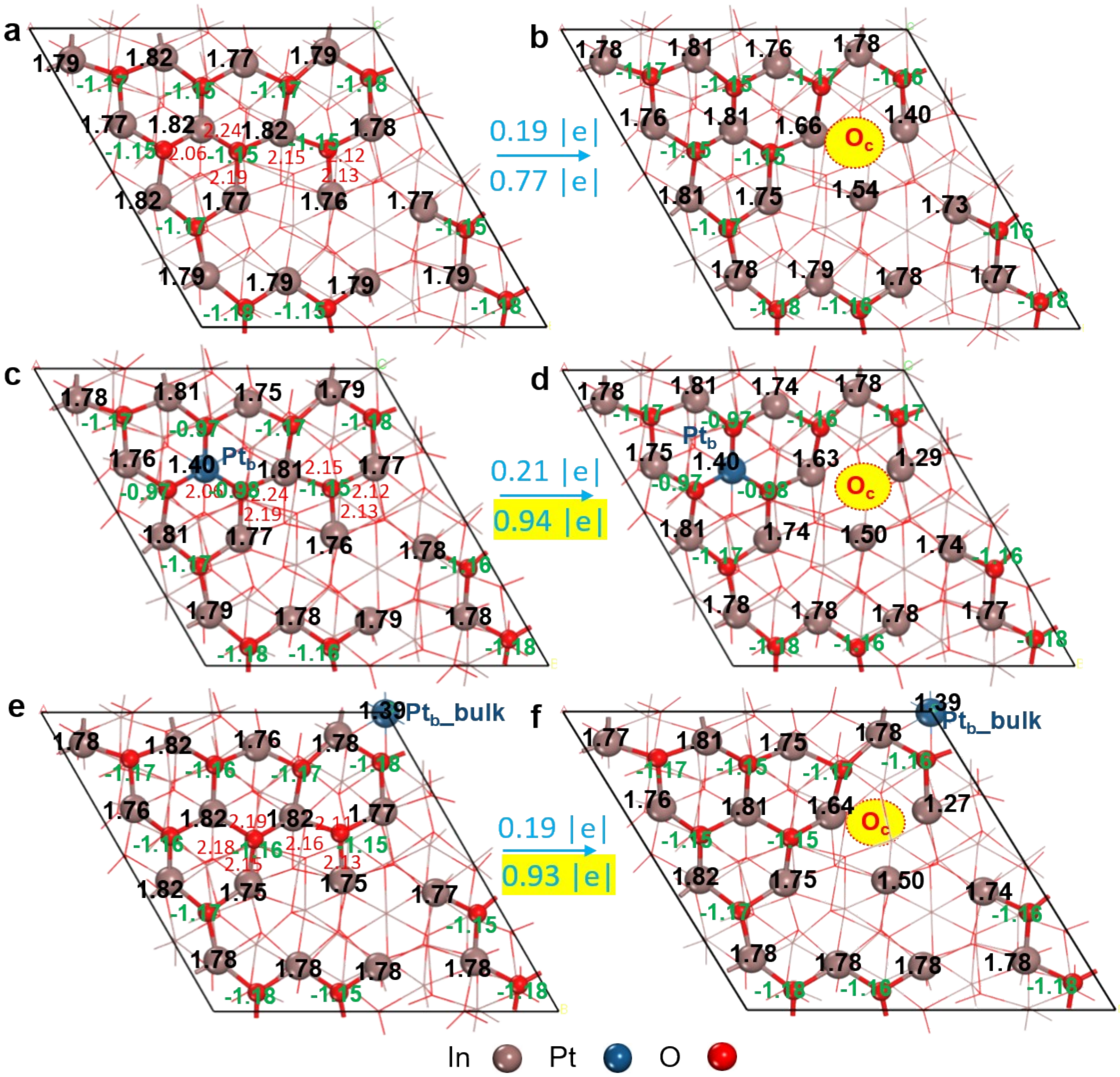

Figure S3. Calculated Bader charges of pristine In_2O_3(111) (**a**), surface-doped Pt/In_2O_3 (**c**) and bulk-doped Pt/In_2O_3 (**e**) and those structures with the O_{c_vac} site (**b**, **d**, **f**), where values in black are the positive charges of the surface metal sites (In/Pt), and values in green are the negative charges of the surface O sites (values in red are the metal-oxygen bond lengths in Å). The numbers above the blue arrows represent the total amount of charges transferred from the In_6, In_7, and In_{10} sites after V_O formation, whereas the numbers below the blue arrows represent those transferred from the In_7, In_8, and In_{11} sites after V_O formation.

To rationalize the effect of introducing the Pt dopant on the $\Delta G_{f,VO}$ value of a given V_O site such as the O_{b_vac} or O_{c_vac} site on the $In_2O_3(111)$ surface, we calculated the atomic charges via Bader charge analysis [1, 2] as shown in Figure S2 and Figure S3. When the Pt dopant substitutes the $In_{b\_surface}$ site, the positive charge of the resulting $Pt_{b\_surface}$ site is significantly lower at 1.40 |e| than the $In_{b\_surface}$ site of 1.82 |e|, which results in the much less negative charges of the surrounding three O atoms of −0.97 |e|, compared with the values of −1.15 |e| before the substitution. Similarly, when the Pt dopant replaces the In_{b_bulk} site, the charges on the six O sites surrounding the Pt dopant changes from −1.23 |e| to about −1.07 |e|, whereas the charges on all the surface metal and O atoms remain nearly unchanged. For the formation of the O_{b_vac} site (Figure S2), the introduction of the $Pt_{b\_surface}$ dopant leads to the deeper reduction of the three metal sites around the O_{b_vac} site as reflected from the greater decrease in the sum of their positive charges, 0.79 |e| after Pt doping versus 0.34 |e| before Pt doping. Deeper reduction of the three metal sites suggests lower stability, which is consistent with the increase in the $\Delta G_{f,VO}$ value from −0.59 eV to −0.21 eV upon introducing the $Pt_{b\_surface}$ dopant. Similarly, introducing the Pt_{b_bulk} dopant also leads to the deeper reduction of the three metal sites around the O_{b_vac} site albeit to a less extent as indicated by the decrease in the sum of their positive charges of 0.55 |e|, consistent with the further increase in the $\Delta G_{f,VO}$ value to −0.06 eV. For the formation of the O_{c_vac} site (Figure S3), introducing the Pt dopant at the $In_{b\_surface}$ (In_{b_bulk}) site always leads to the deeper reduction of the three metal sites around the O_{c_vac} site, as the decrease in the sum of their positive charges increases from 0.77 |e| before Pt doping to 0.94 |e| (0.93 |e|) after Pt doping at the $In_{b\_surface}$ (In_{b_bulk}) site, respectively, consistent with the increase in the $\Delta G_{f,VO}$ value from −0.08 eV to 0.20 eV (0.15 eV).

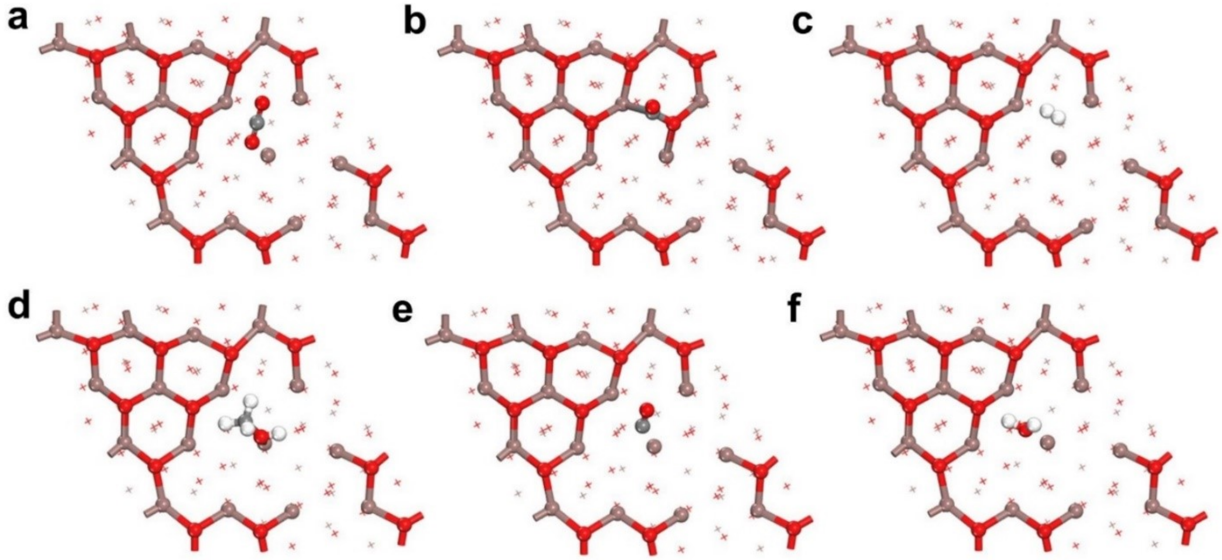

Figure S4. **Optimized structures of important adsorbates on the pristine In_2O_3(111) surface**. (**a-f**) Optimized structures of ln-CO_2 (**a**), bt-CO_2 (**b**), H_2 (**c**), CH_3OH (**d**), CO (**e**), and H_2O (**f**) at the O_{c_vac} site on the defective In_2O_3(111) surface.

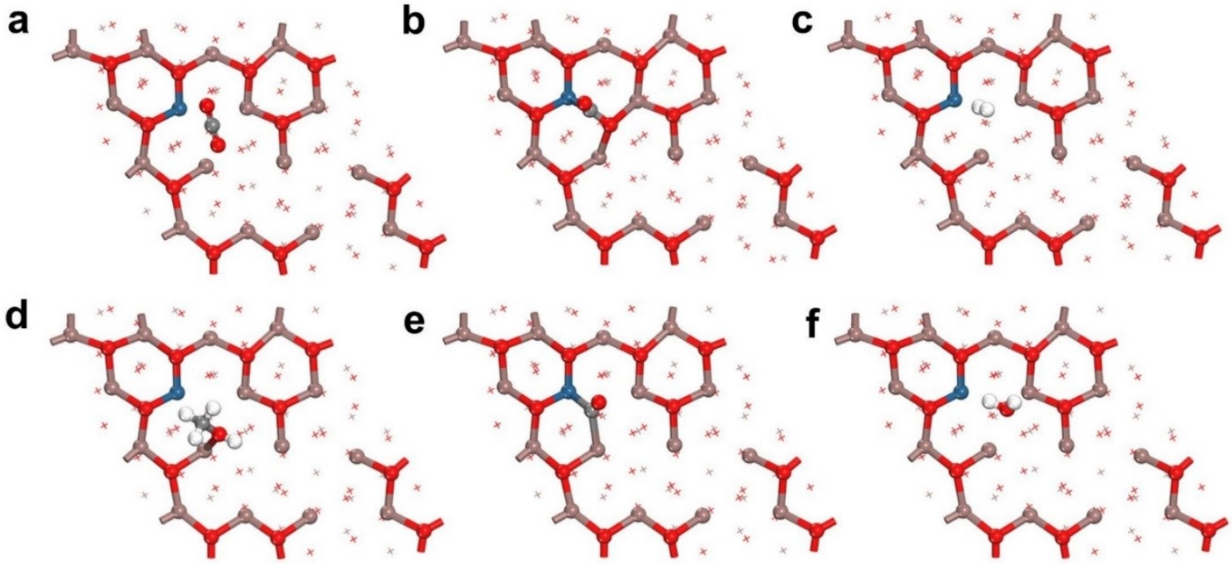

Figure S5. **Optimized structures of important adsorbates on the surface-doped Pt/In_2O_3(111) model**. (**a-f**) Optimized structures of ln-CO_2 (**a**), bt-CO_2 (**b**), H_2 (**c**), CH_3OH (**d**), CO (**e**), and H_2O (**f**) at the $Pt_{b\_surface}$-O_{b_vac} site on the surface-doped Pt/In_2O_3(111) model.

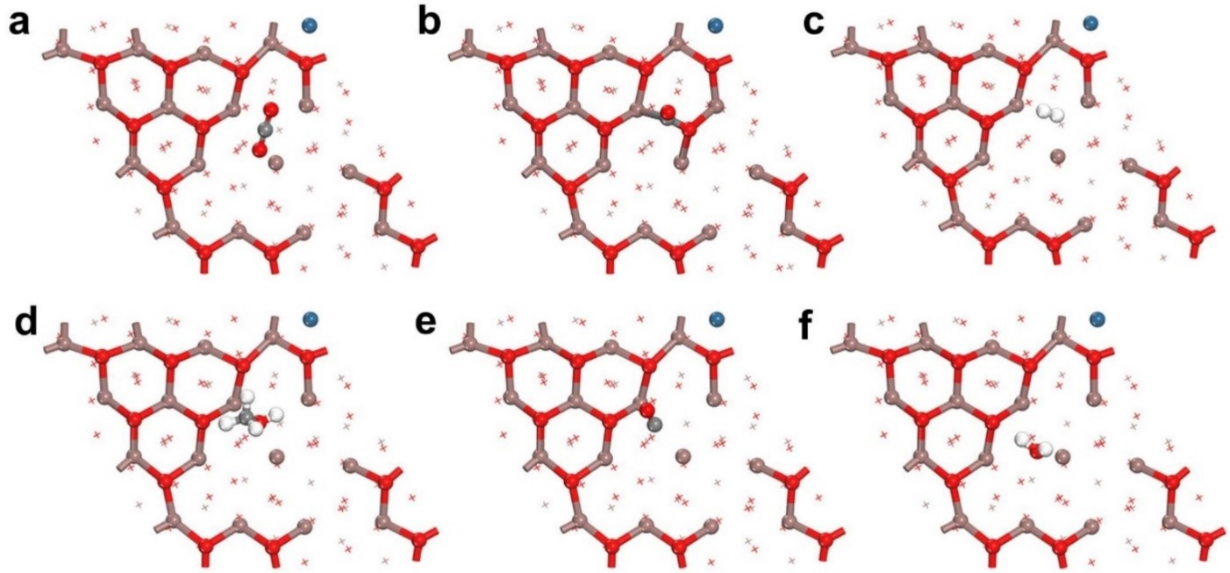

Figure S6. **Optimized structures of important adsorbates on the bulk-doped Pt/In_2O_3(111) model**. (**a-f**) Optimized structures of ln-CO_2 (**a**), bt-CO_2 (**b**), H_2 (**c**), CH_3OH (**d**), CO (**e**), and H_2O (**f**) at the Pt_{b_bulk}-O_{c_vac} site on the bulk-doped Pt/In_2O_3(111) model.

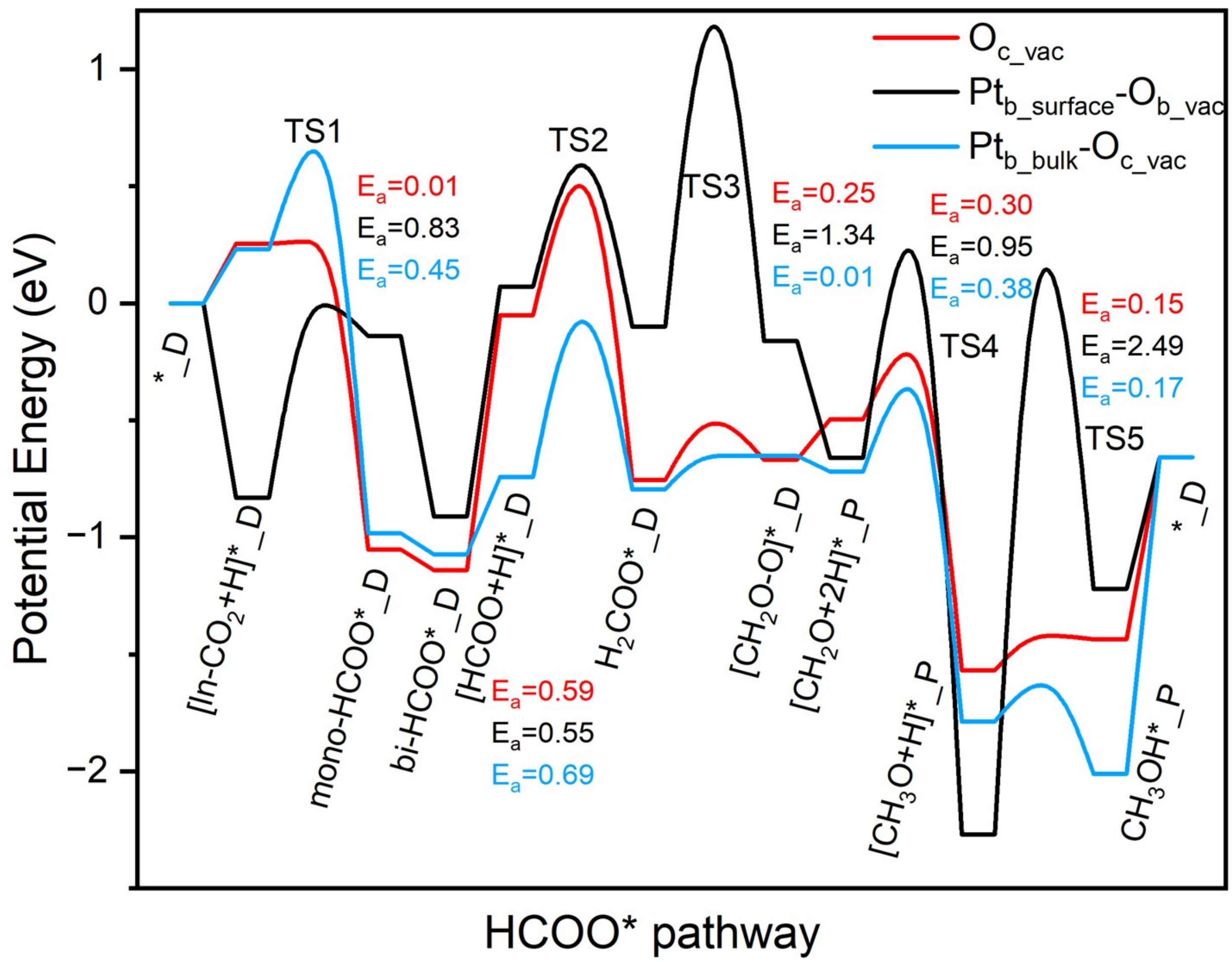

Figure S7. **Energy profiles for CH_3OH formation via the HCOO pathway**. Relative energies in eV (electronic energies only) are shown for CO_2 hydrogenation to CH_3OH via the HCOO pathway at the O_{c_vac} site on the defective $In_2O_3(111)$ surface (red), at the $Pt_{b\_surface}$-O_{b_vac} site on the surface-doped $Pt/In_2O_3(111)$ model (black), and at the Pt_{b_bulk}-O_{c_vac} site on the bulk-doped $Pt/In_2O_3(111)$ model (blue).

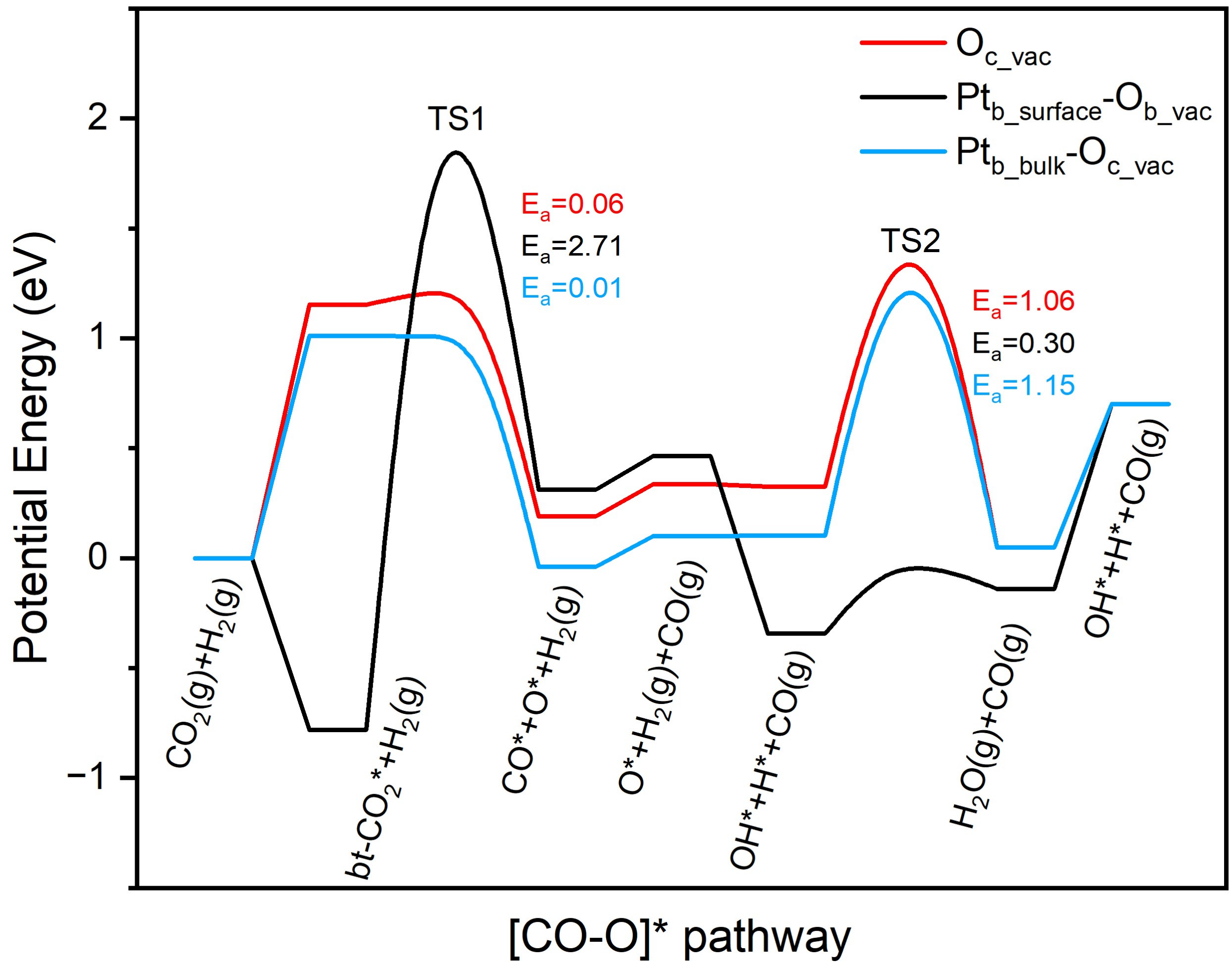

Figure S8. **Energy profiles for CO formation by direct CO_2 dissociation**. Relative energies in eV (electronic energies only) are shown for CO_2 direct dissociation to CO at the O_{c_vac} site on the defective $In_2O_3(111)$ surface (red), at the $Pt_{b\_surface}$-O_{b_vac} site on the surface-doped Pt/$In_2O_3(111)$ model (black), and at the Pt_{b_bulk}-O_{c_vac} site on the bulk-doped Pt/$In_2O_3(111)$ model (blue).

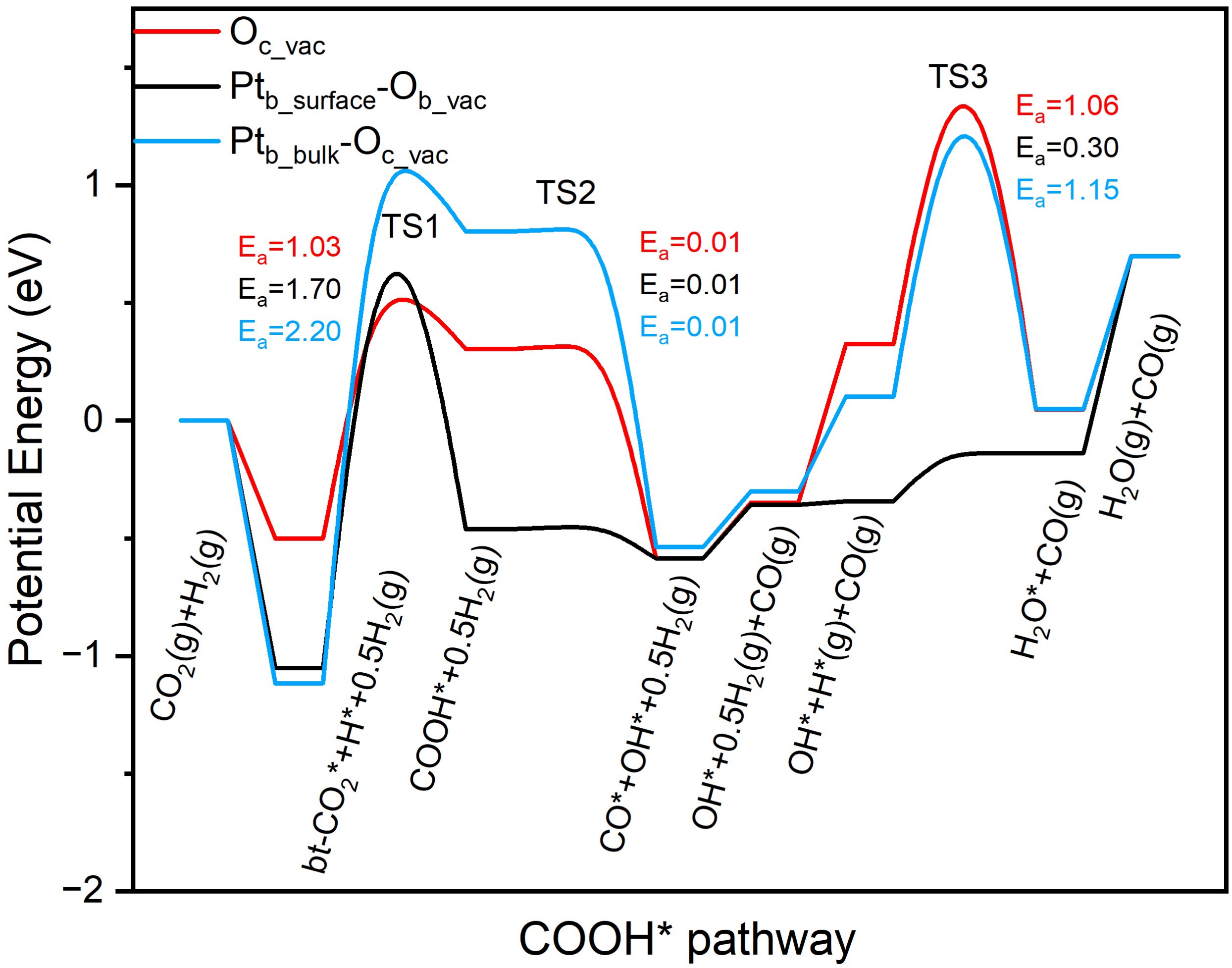

Figure S9. **Energy profiles for CO formation via the COOH pathway**. Relative energies in eV (electronic energies only) are shown for CO_2 hydrogenation to CO via the indirect COOH pathway at the O_{c_vac} site on the defective $In_2O_3(111)$ surface (red), at the $Pt_{b\_surface}$-O_{b_vac} site on the surface-doped $Pt/In_2O_3(111)$ model (black), and at the Pt_{b_bulk}-O_{c_vac} site on the bulk-doped $Pt/In_2O_3(111)$ model (blue).

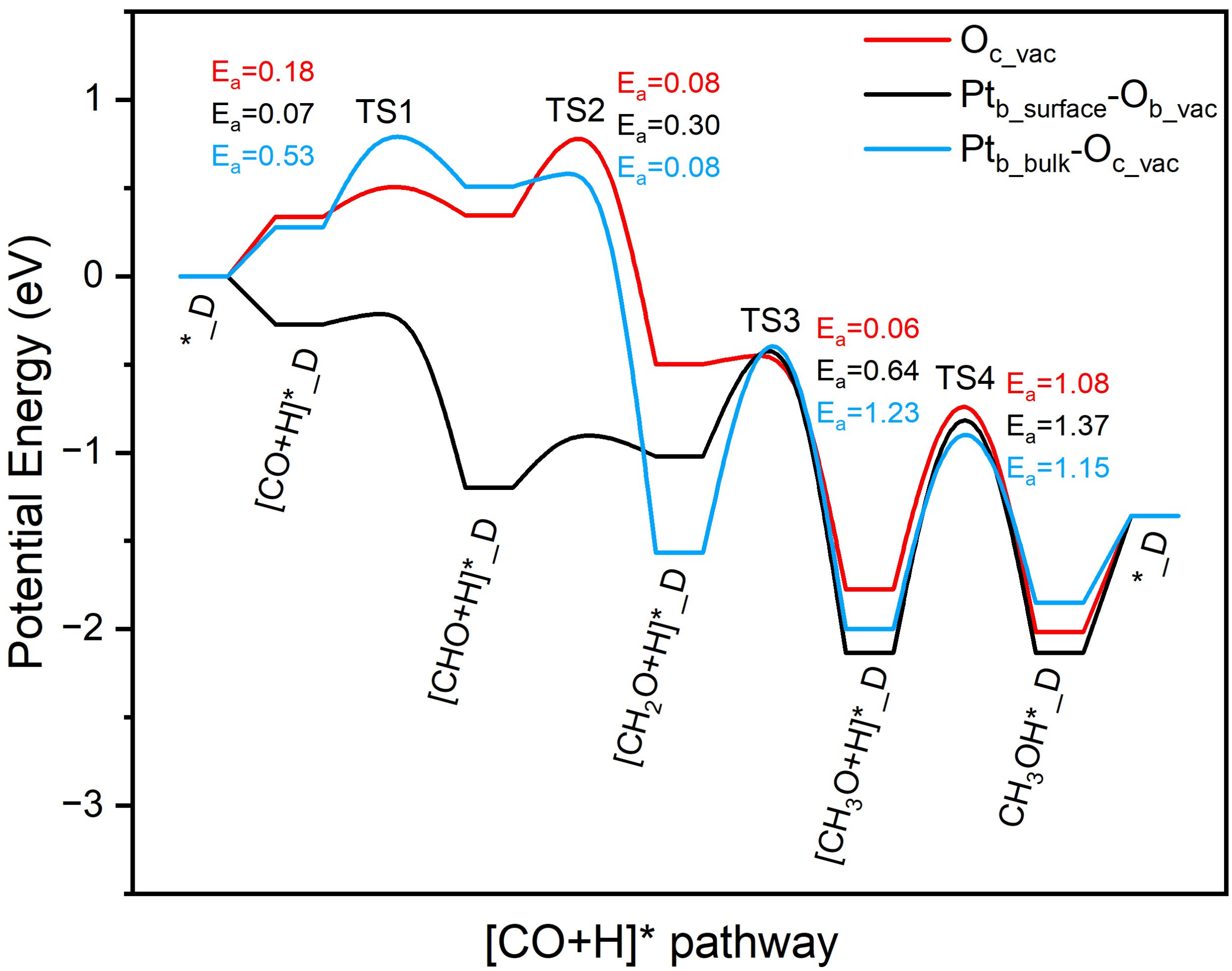

Figure S10. **Energy profiles for CH_3OH formation via the CO hydrogenation pathway**. Relative energies in eV (electronic energies only) are shown for CO hydrogenation to CH_3OH at the O_c_vac site on the defective $In_2O_3(111)$ surface (red), at the $Pt_{b\_surface}$-O_{b_vac} site on the surface-doped Pt/$In_2O_3(111)$ model (black), and at the Pt_{b_bulk}-O_{c_vac} site on the bulk-doped Pt/$In_2O_3(111)$ model (blue).

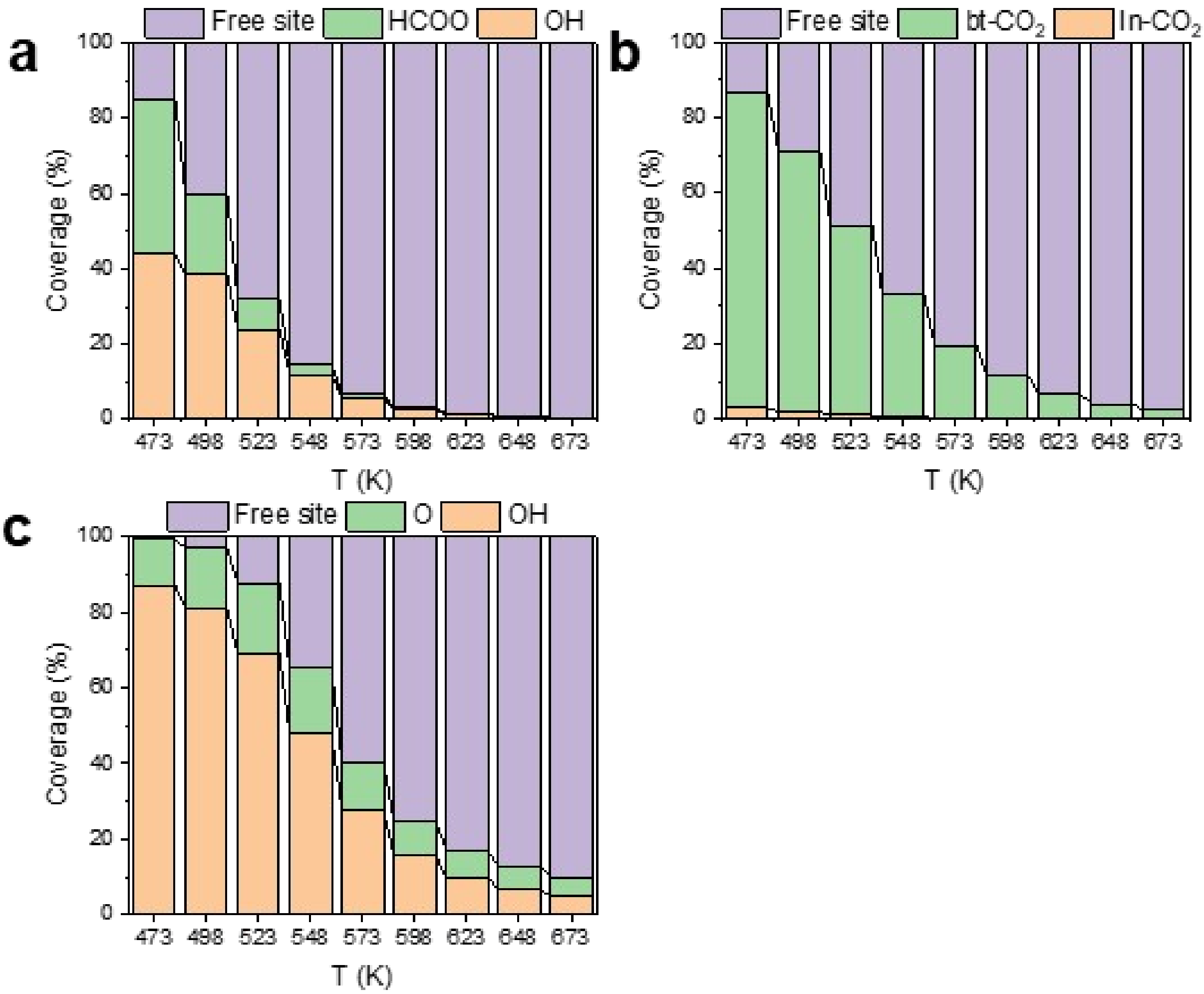

Figure S11. **Calculated coverages of surface adsorbates**. (**a-c**) Coverages of the major surface species during the CO_2 hydrogenation reaction at the O_{c_vac} site on the defective $In_2O_3(111)$ surface (**a**), at the $Pt_{b\_surface}$-O_{b_vac} site on the surface-doped Pt/$In_2O_3(111)$ model (**b**), and at the Pt_{b_bulk}-O_{c_vac} site on the bulk-doped Pt/$In_2O_3(111)$ model (**c**).

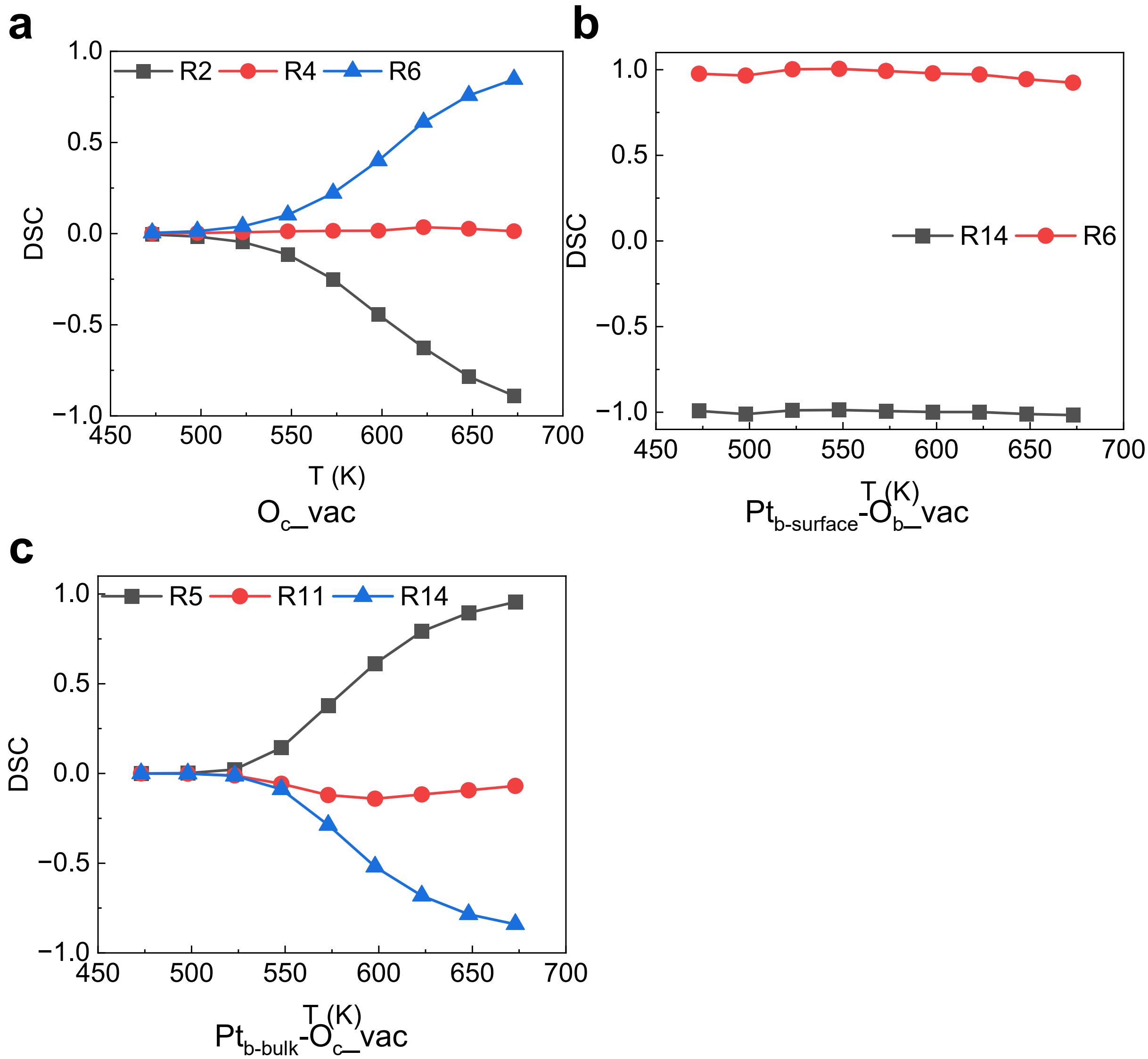

Figure S12. **Calculated degrees of selectivity control for CH_3OH**. (**a-c**) Degrees of selectivity control for CH_3OH (DSC) during the CO_2 hydrogenation reaction at the O_{c_vac} site on the defective In_2O_3(111) surface (**a**), at the $Pt_{b\_surface}$-O_{b_vac} site on the surface-doped Pt/In_2O_3(111) model (**b**), and at the Pt_{b_bulk}-O_{c_vac} site on the bulk-doped Pt/In_2O_3(111) model (**c**).

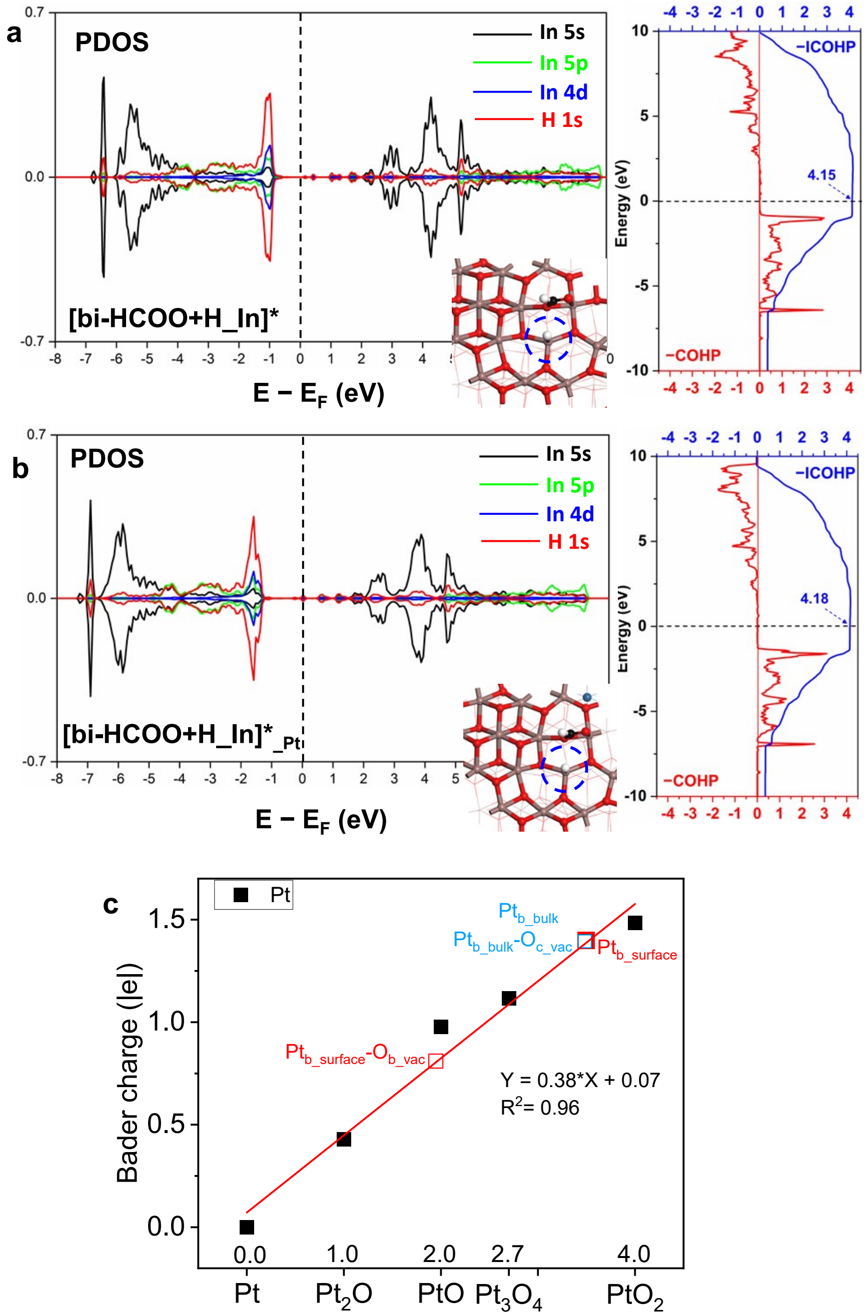

Figure S13. Electronic structure analysis and estimation of formal oxidation states. (a,b) Projected Density of State (PDOS) and Crystal Orbital Hamilton Population (COHP) analyses for the interaction between the In site and the H adsorbate in the presence of HCOO* at the oxygen vacancy for the In_2O_3(111) and bulk-doped Pt/In_2O_3 (Pt_{b_bulk}) models. Integrated COHP (ICOHP) values at the Fermi energy indicate the strength of the In-H interaction. (c) Estimation of the formal oxidation states of the Pt single atom sites based on the linear relationship between the calculated Bader charges and formal oxidation states of bulk Pt and its oxides.

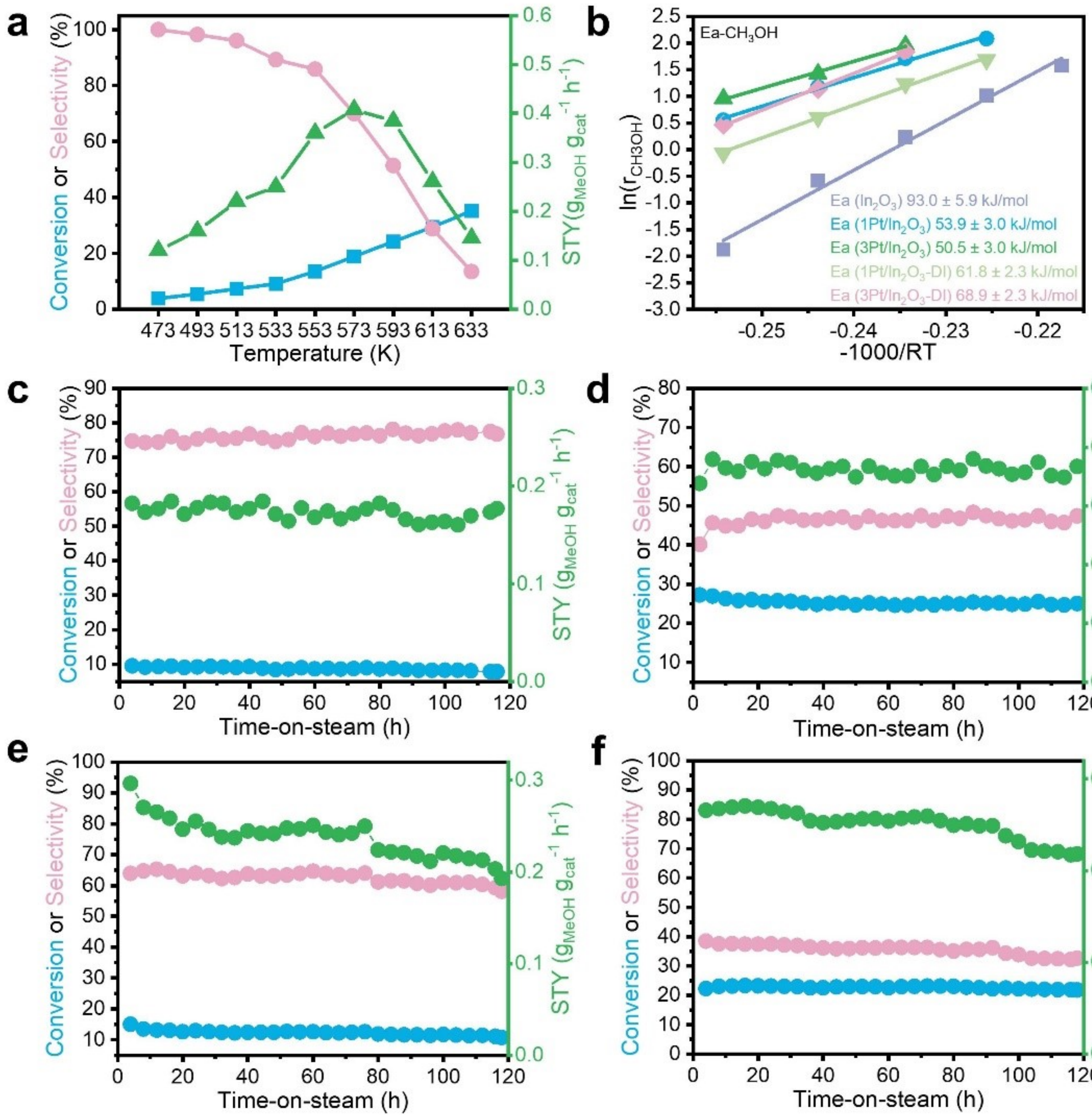

Figure S14. The catalytic performance of the catalysts. (**a**) Effects of temperature on CO_2 hydrogenation over 1Pt/In_2O_3 catalyst. (**b**) Arrhenius plots and activation energies of methanol synthesis reactions over In_2O_3 and Pt modified In_2O_3 by different method. (**c-f**) Stability test of In_2O_3 (**c**), 3Pt/In_2O_3 (**d**), 1Pt/In_2O_3-DI (**e**), and 3Pt/In_2O_3-DI (**f**). Standard reaction conditions: 5 MPa, 573 K, H_2, H_2/CO_2 = 3:1, GHSV = 9000 mL·g_{cat}^{-1}·h^{-1}.

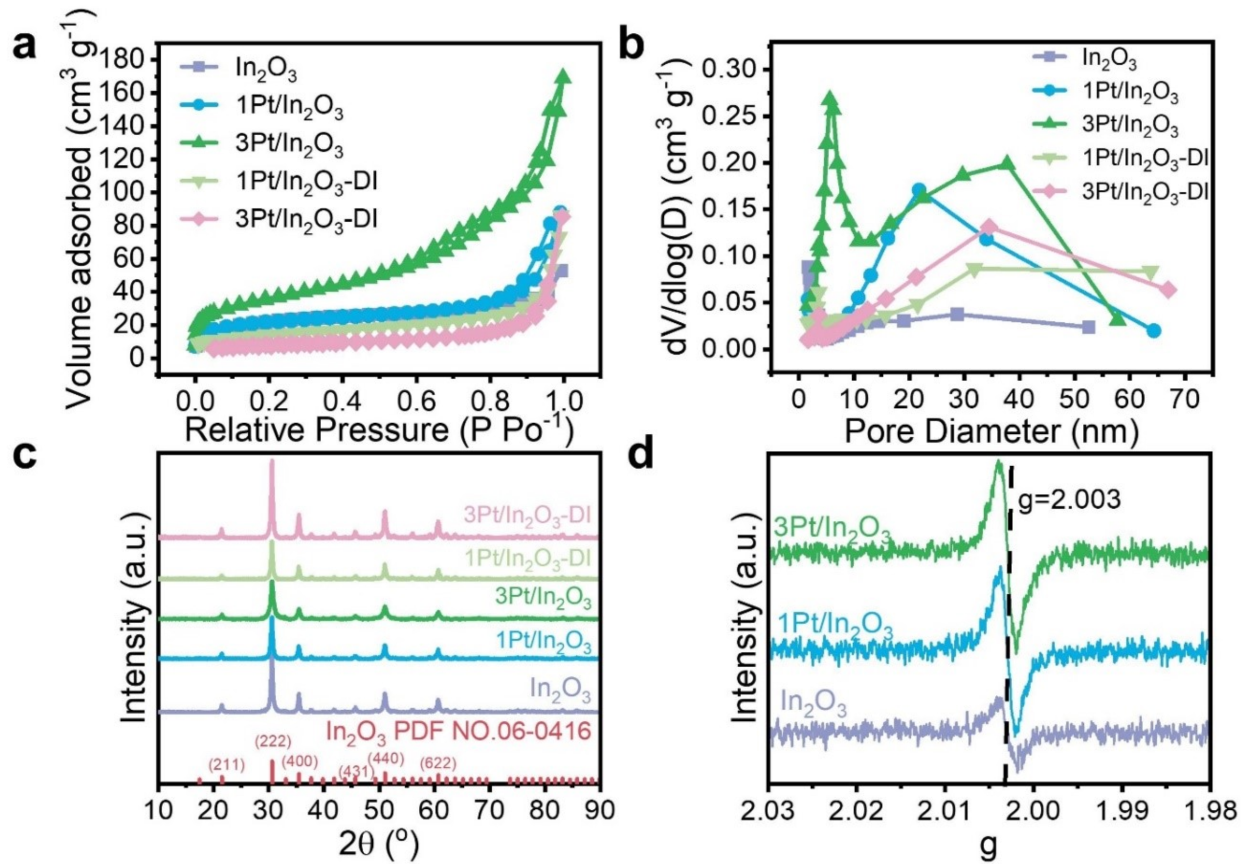

Figure S15. Characterization of various catalysts. (**a-d**) N_2 adsorption-desorption isotherms (**a**), pore size distribution (**b**), XRD patterns (**c**) and EPR spectra (**d**) of In_2O_3 and various Pt modified In_2O_3 catalysts.

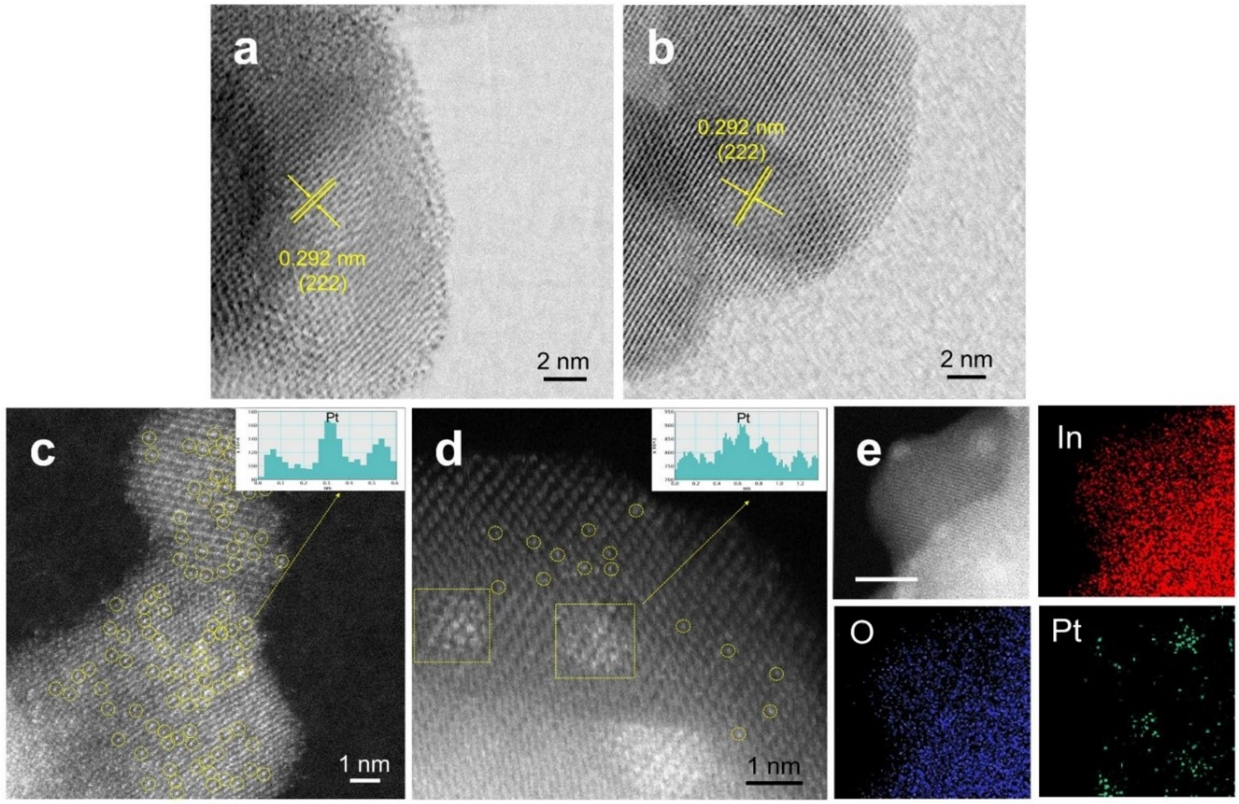

Figure S16. Characterization of the samples. (**a,b**) HRTEM images of $1Pt/In_2O_3$ (**a**) and $3Pt/In_2O_3$ (**b**). (**c,d**) HAADF-STEM images of $3Pt/In_2O_3$ spent for 48h (**c**) and $1Pt/In_2O_3$-DI spent for 48h (**d**), line-scanning intensity profiles (inlet) obtained on the zoomed areas. (**e**) TEM-EDS elemental mapping of $1Pt/In_2O_3$-DI catalyst spent for 48 h, scale bar, 10 nm.

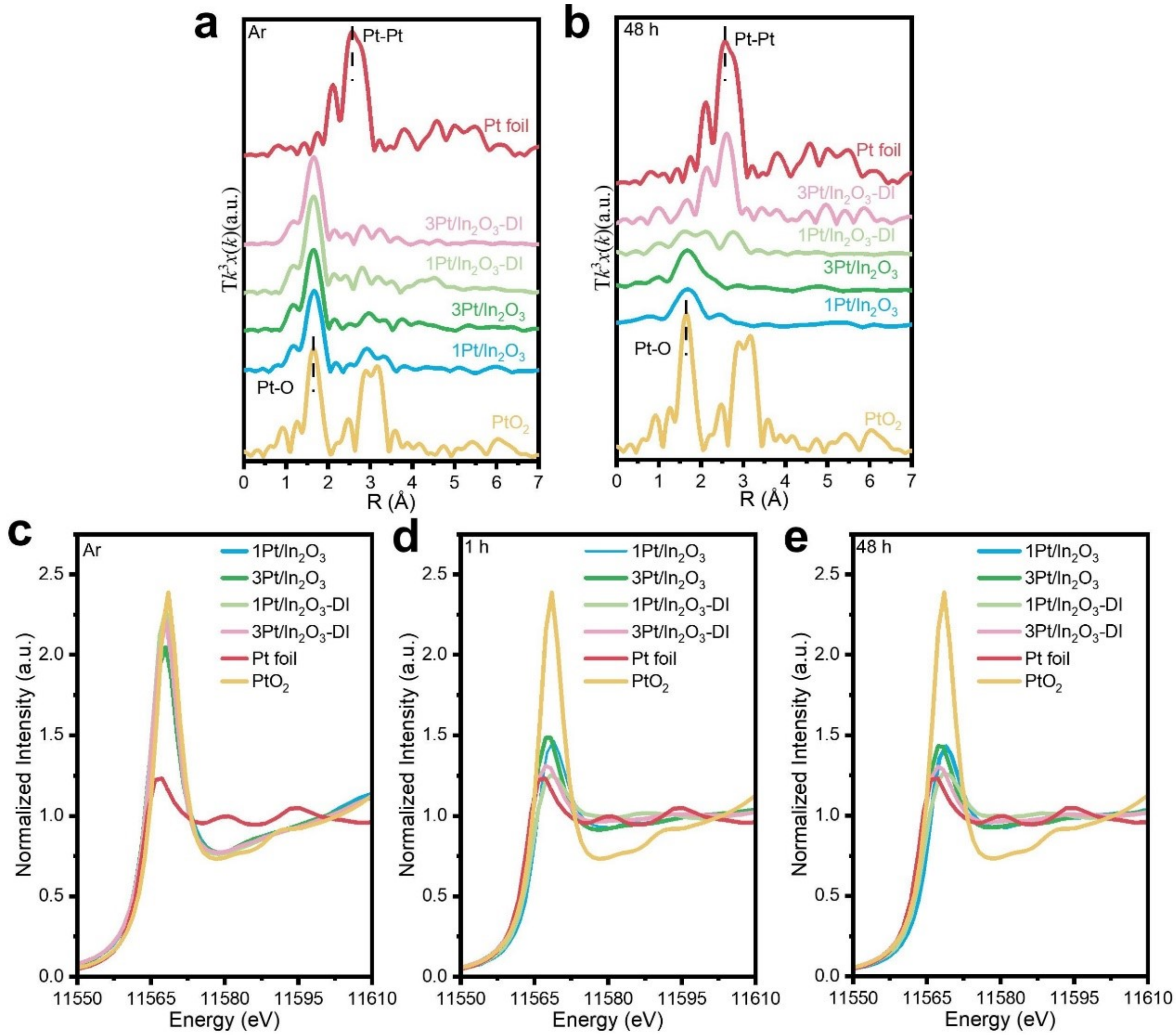

Figure S17. X-ray absorption studies. (**a,b**) The k^3-weighted Fourier transform of the EXAFS spectra of catalysts pretreated in Ar at 573 K for 1 h (**a**), and after the CO_2 hydrogenation reaction for 48 h (**b**). (**c-f**) Normalized XANES spectra at the Pt L_3-edge of Pt foil, PtO_2, and various Pt modified In_2O_3 catalysts pretreated in Ar at 573 K for 1 h (**c**), and after the CO_2 hydrogenation reaction for 1 h (**d**) and 48 h (**e**).

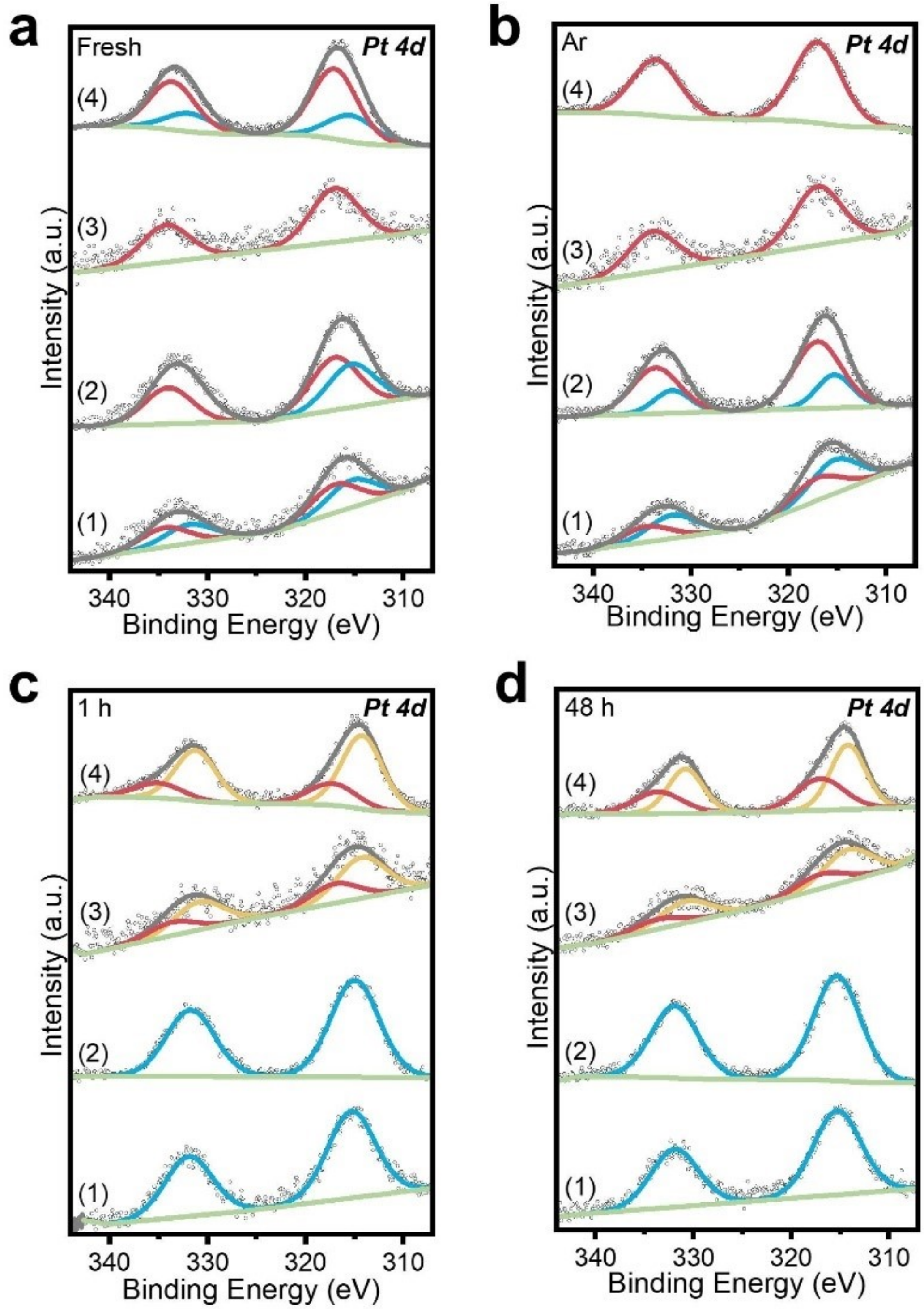

Figure S18. XPS results. (**a-d**) XPS spectra of Pt 4d for fresh samples (**a**), samples pretreated in Ar at 573 K for 1 h (**b**) and catalysts after CO_2 hydrogenation reaction for 1 h (**c**) or 48 h (**d**). (1) In_2O_3, (2) $1Pt/In_2O_3$, (3) $3Pt/In_2O_3$, (4) $1Pt/In_2O_3$-DI, (5) $3Pt/In_2O_3$-DI.

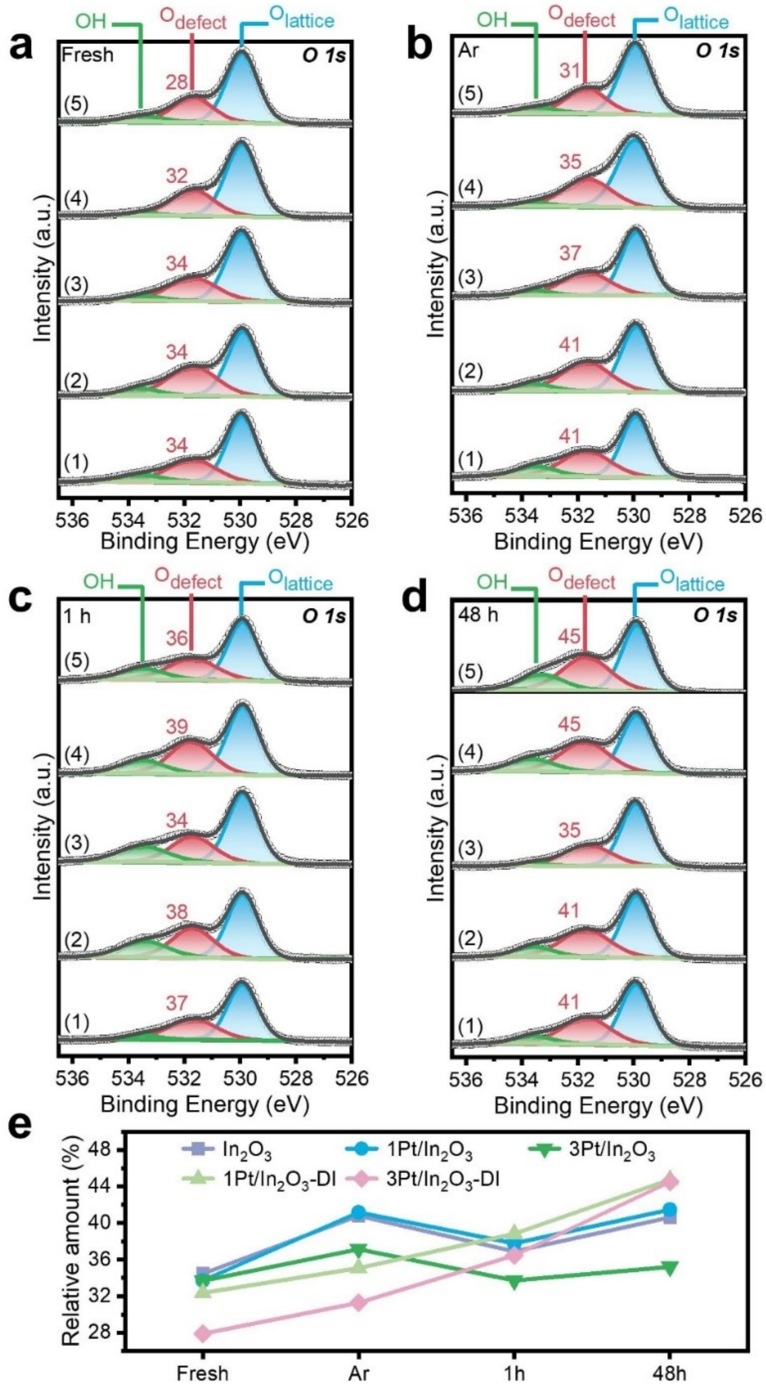

Figure S19. XPS results. (**a-d**) XPS spectra of O 1s for fresh samples (**a**), samples pretreated in Ar at 573 K for 1 h (**b**), and catalysts after CO_2 hydrogenation reaction for 1 h (**c**) or 48 h (**d**). (**e**) The relative oxygen vacancy concentration of samples with different situation. (1) In_2O_3, (2) $1Pt/In_2O_3$, (3) $3Pt/In_2O_3$, (4) $1Pt/In_2O_3$-DI, (5) $3Pt/In_2O_3$-DI.

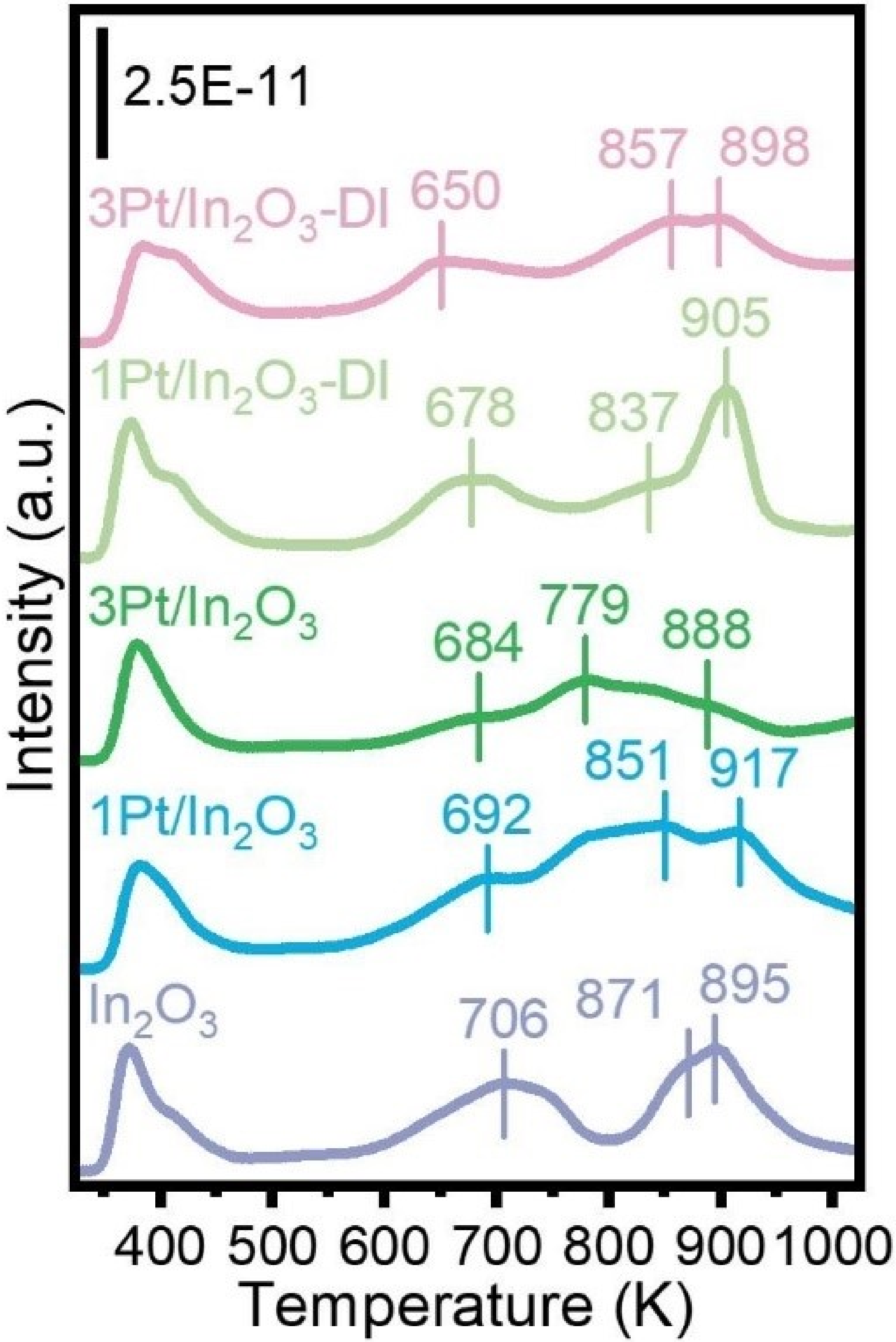

Figure S20. CO_2-TPD profiles. Pristine In_2O_3 and various Pt modified In_2O_3 catalysts were pretreated in 5%H_2/Ar at 573 K for 1 h.

R1:CO2_g + *_s <-> CO2_s #ln-CO2

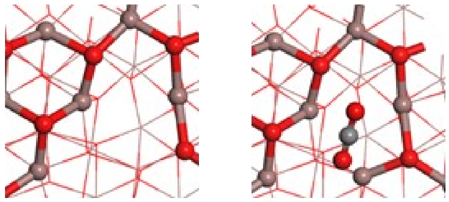

R2:CO2_g + *_s <-> O2C_s #bt-CO2

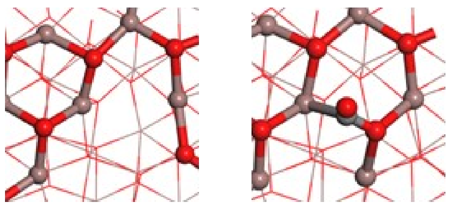

R3:CO2_s + H_h <-> [CO2-H_s] + *_h <-> HCOO_s + *_h

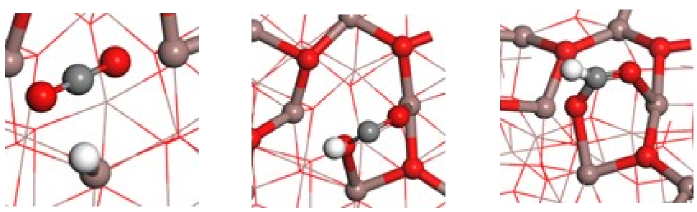

R4:HCOO_s + H_h <-> [HCOO-H_s] + *_h <-> H2COO_s + *_h

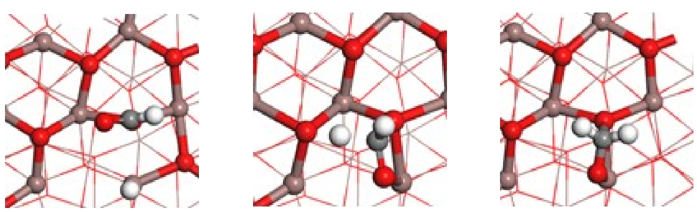

R5:H2COO_s <-> [H2CO-O_s] <-> OH2CO_s

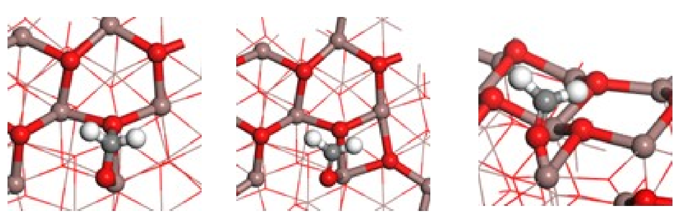

R6:OH2CO_s + 2H_h <-> [OHH2CO-H_s] + 2*_h <-> OH3COH_s + 2*_h

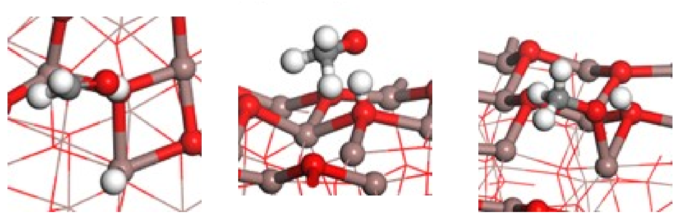

R7:OH3COH_s <-> [OH3CO-H_s] <-> OCH3OH_s

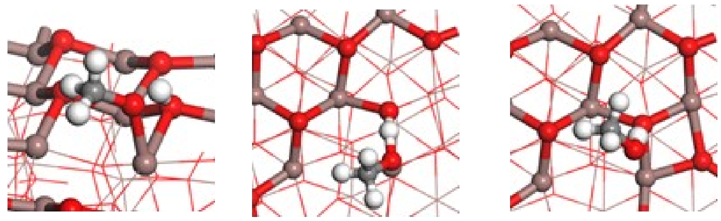

R8:OCH3OH_s <-> CH3OH_g + O_s

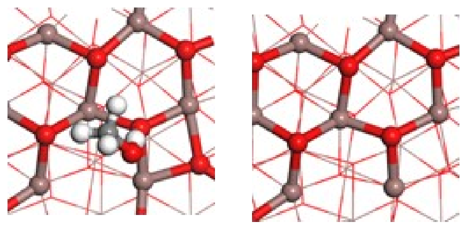

R9:H2_g + 2*_h <-> [H-H_h] + *_h <-> 2H_h

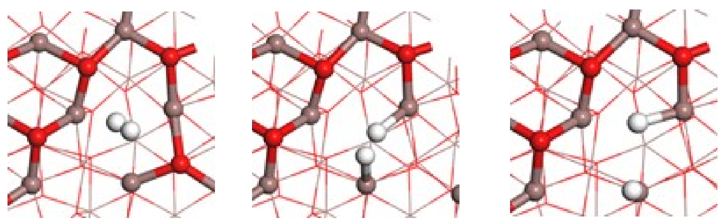

R10:H2_g + O_s + *_h <-> [OH-H_s] + *_h <-> OH_s + H_h

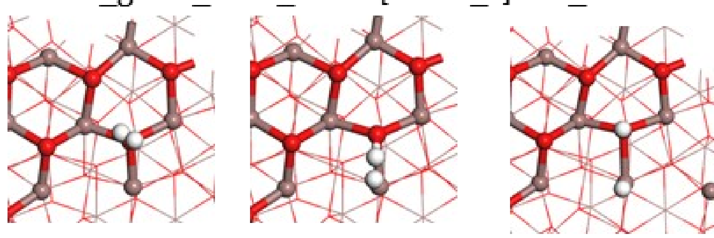

R11:OH_s + H_h <-> [H-OH_s] + *_h <-> H2O_s + *_h

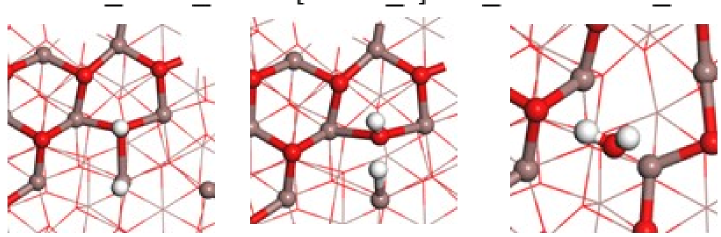

R12:H2O_s <-> H2O_g + *_s

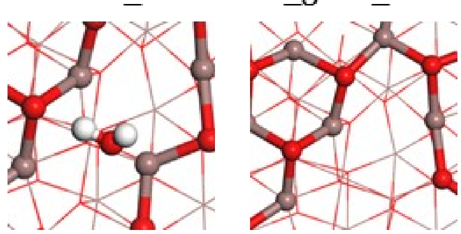

R13:O_s + H_h <-> OH_s + *_h

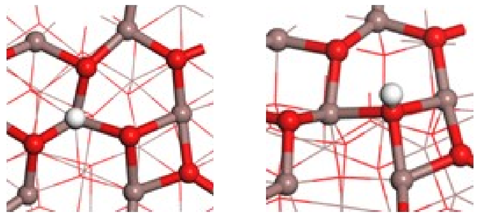

R14:CO2_s + *_s <-> [CO-O_s] + *_s <-> CO_s + O_s

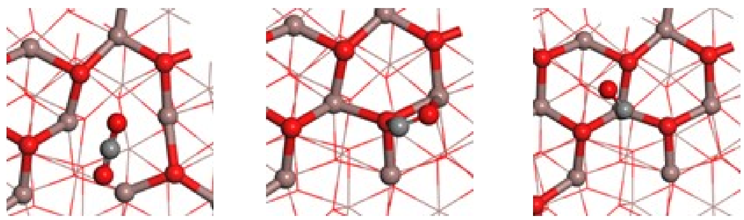

R15:CO_s <-> CO_g + *_s

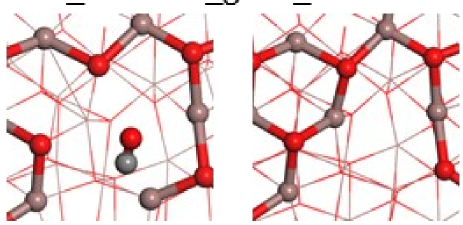

R16:O2C_s + H_h <-> [O2C-H_s] + *_h <-> COOH_s + *_h

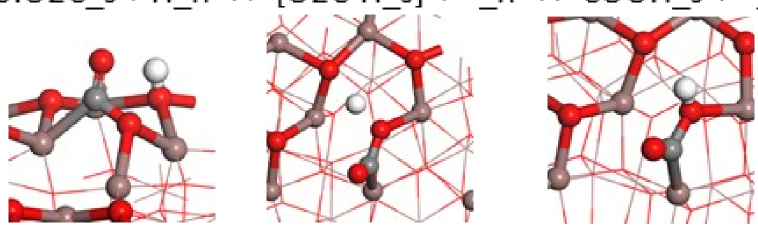

R17:COOH_s + *_s <-> [CO-OH_s] + *_s <-> CO_s + OH_s

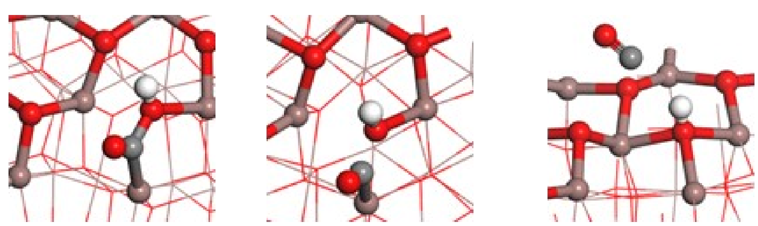

R18:CO_s + H_h <-> [CO-H_s] + *_h <-> CHO_s + *_h

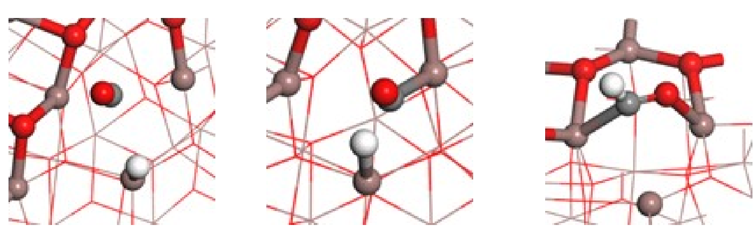

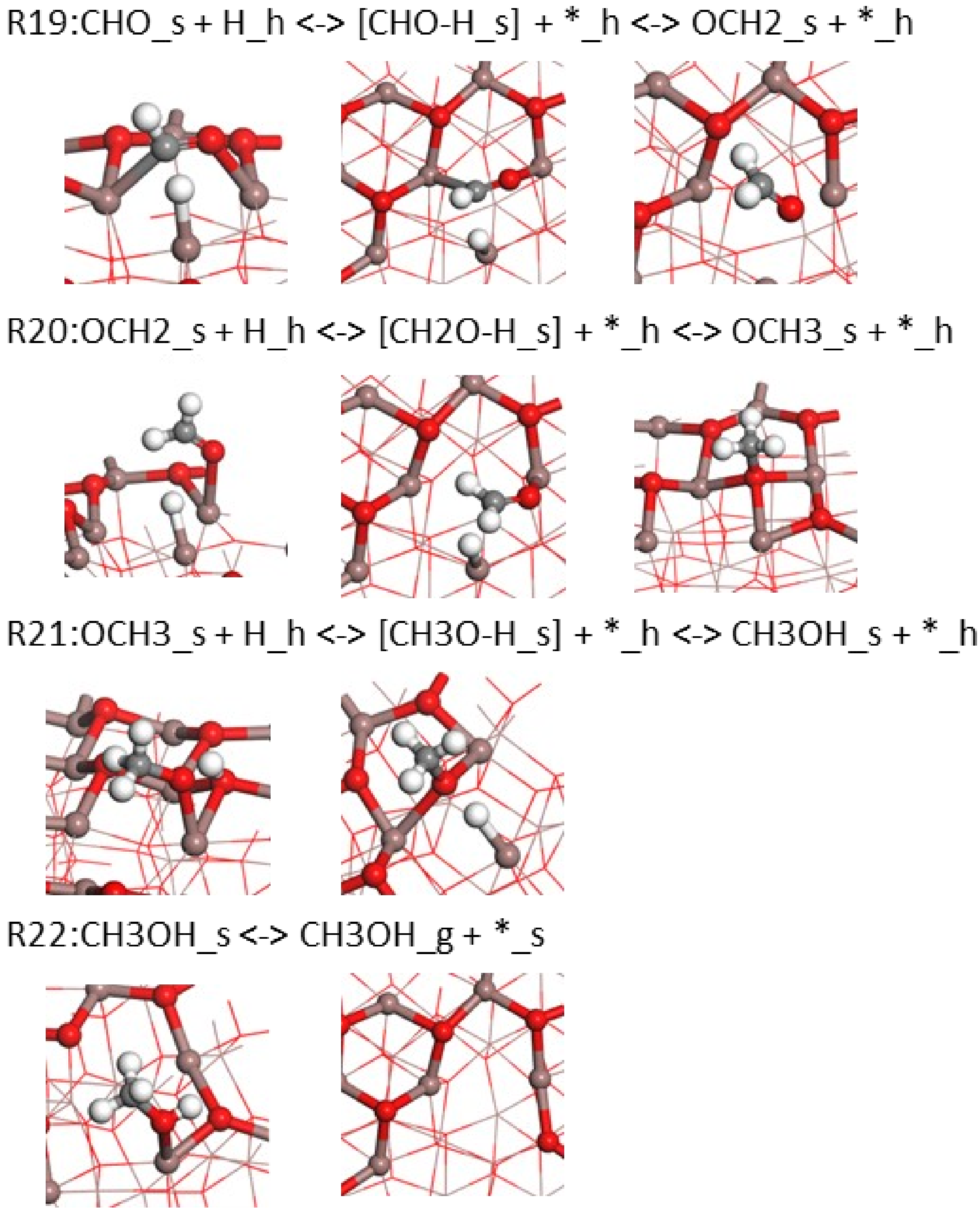

Figure S21. The structures of the intermediates for the elementary steps.

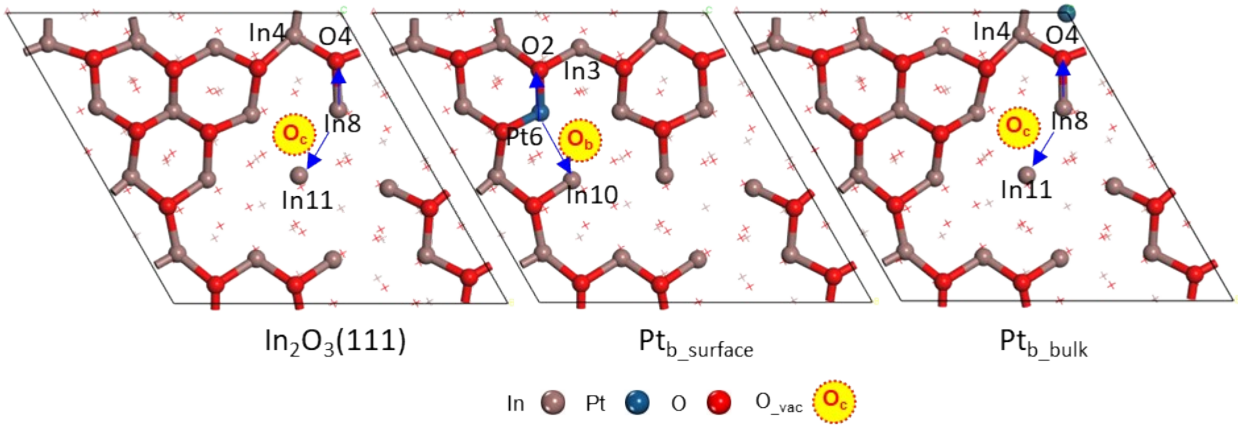

Figure S22. Top view of the structures for H migration for the In_2O_3(111), Pt_{b_bulk} and Pt_{b_bulk} models.

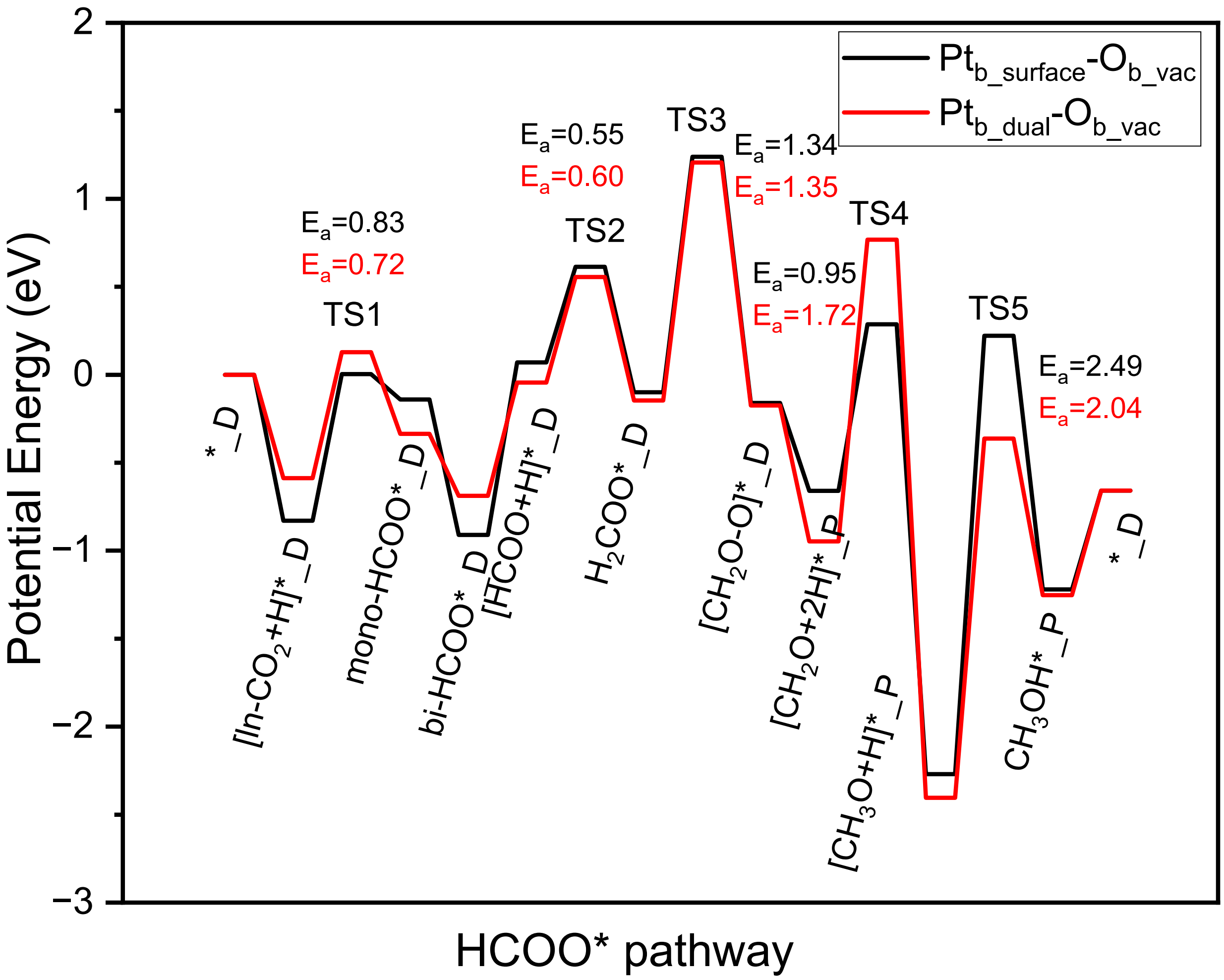

Figure S23. Energy profiles for CH_3OH formation via the HCOO pathway. Relative energies in eV (electronic energies only) are shown for CO_2 hydrogenation to CH_3OH via the HCOO pathway at the $Pt_{b\_surface}$-O_{b_vac} on the surface-doped Pt/In_2O_3(111) model (black), at the Pt_{b_dual}-O_{b_vac} site on the surface and bulk co-doped Pt/In_2O_3(111) model (red).

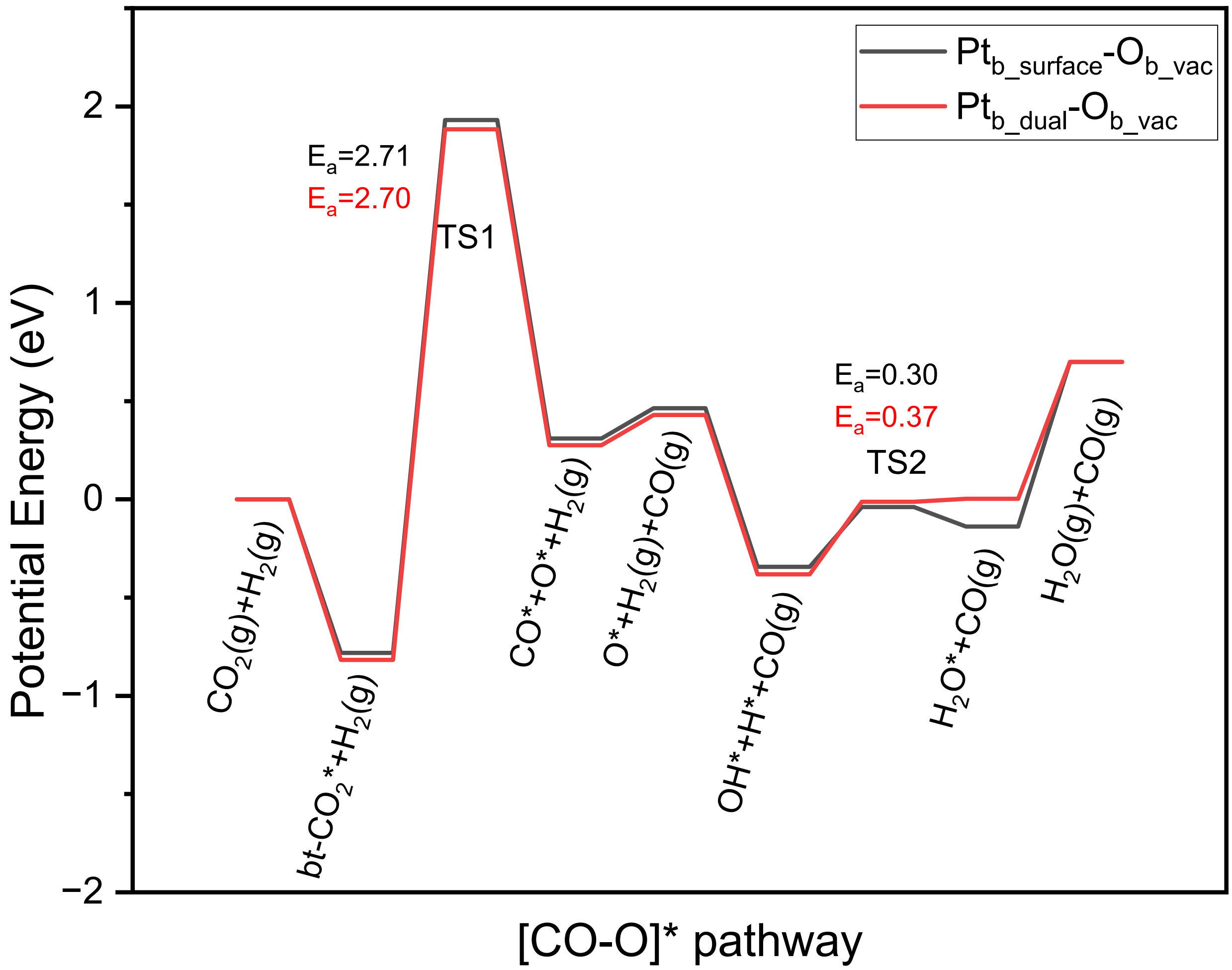

Figure S24. Energy profiles for CO formation by direct CO_2 dissociation. Relative energies in eV (electronic energies only) are shown for CO_2 direct dissociation to CO at the $Pt_{b\_surface}$-O_{b_vac} on the surface-doped Pt/In_2O_3(111) model (black), at the Pt_{b_dual}-O_{b_vac} site on the surface and bulk co-doped Pt/In_2O_3(111) model (red).

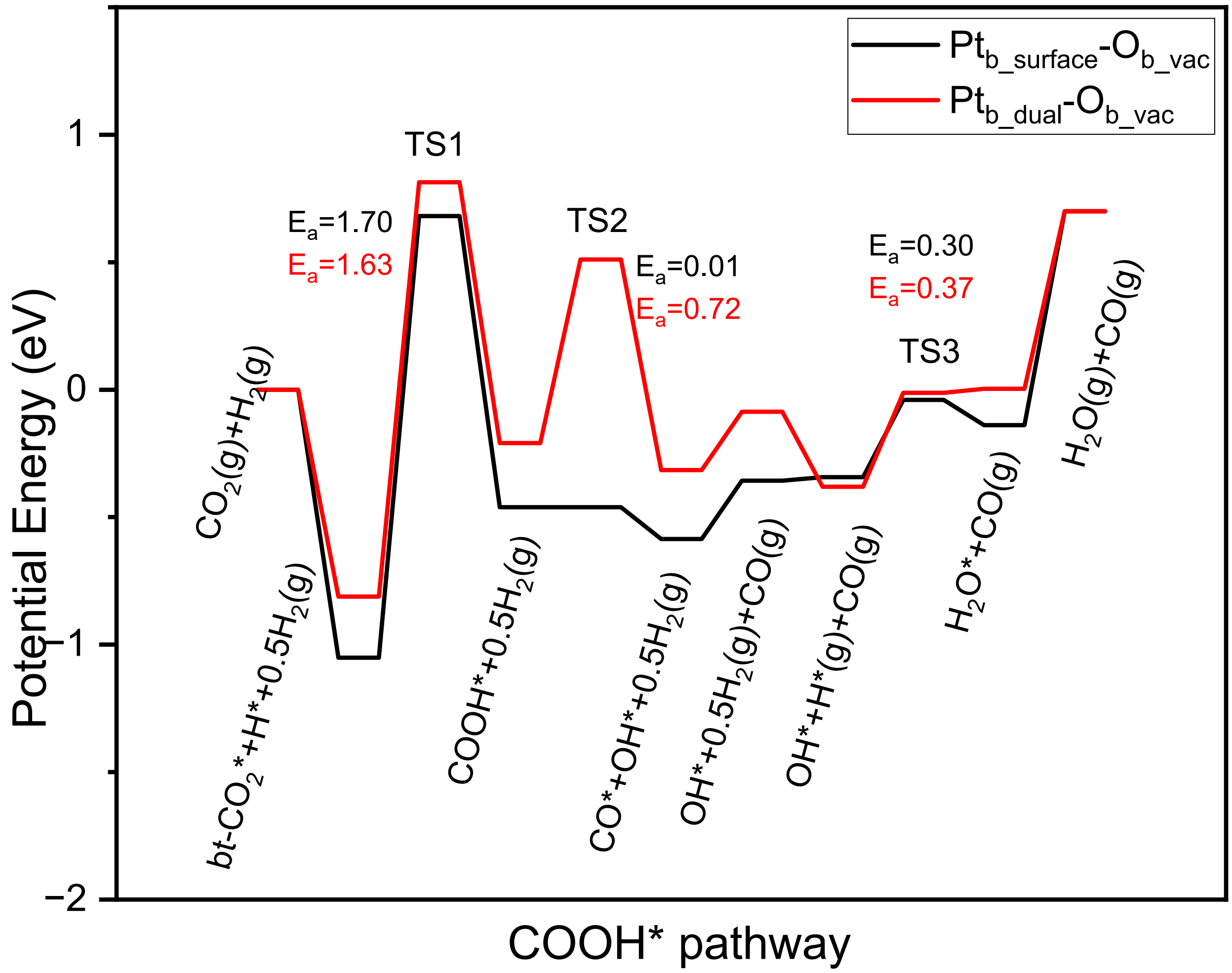

Figure S25. Energy profiles for CO formation via the COOH pathway. Relative energies in eV (electronic energies only) are shown for CO_2 hydrogenation to CO via the indirect COOH pathway at the Pt$_{b_surface}$-O$_{b_vac}$ on the surface-doped Pt/In_2O_3(111) model (black), at the Pt$_{b_dual}$-O$_{b_vac}$ site on the surface and bulk co-doped Pt/In_2O_3(111) model (red).

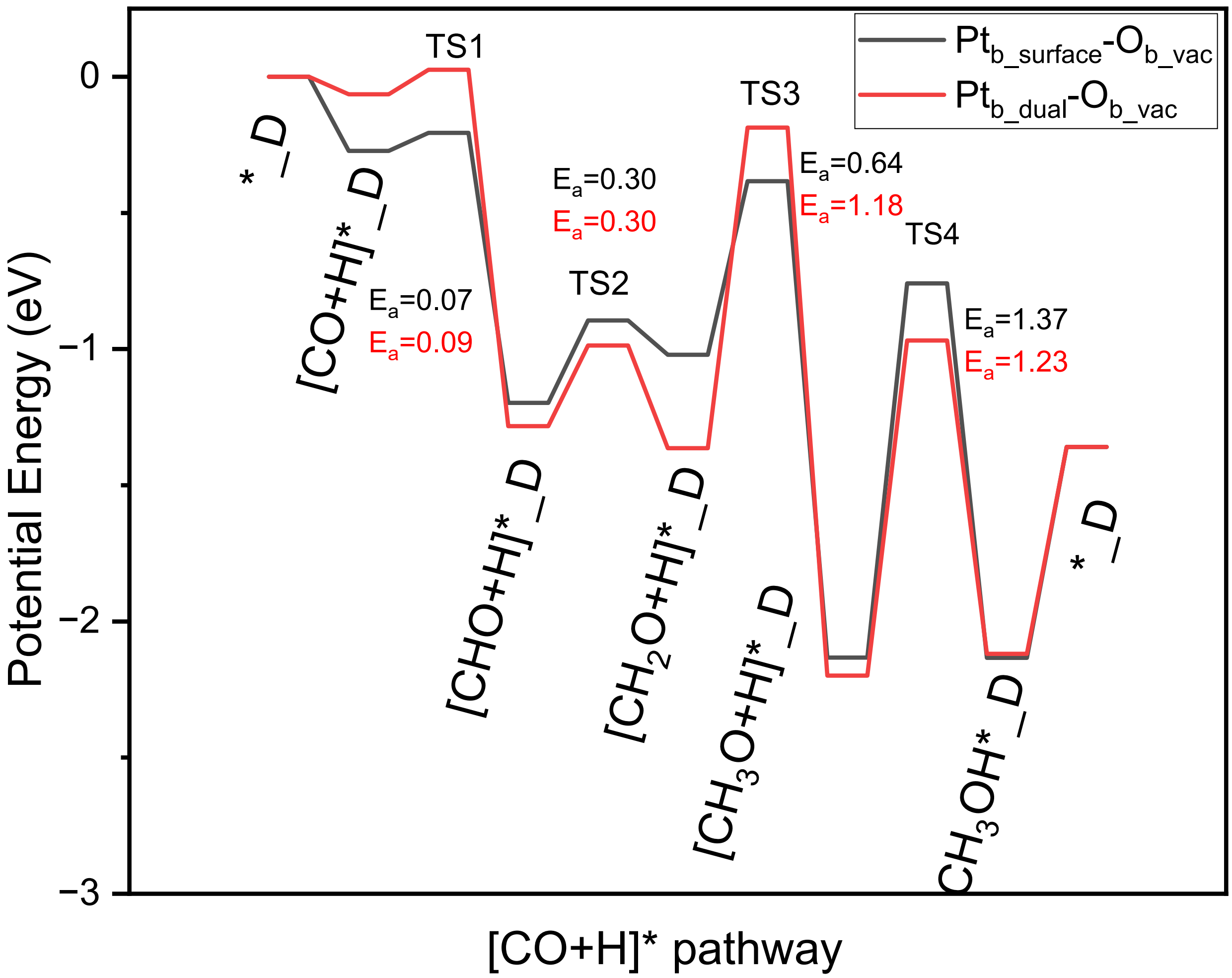

Figure S26. Energy profiles for CH_3OH formation via the CO hydrogenation pathway. Relative energies in eV (electronic energies only) are shown for CO hydrogenation to CH_3OH at the Pt$_{b_surface}$-O$_{b_vac}$ on the surface-doped Pt/In_2O_3(111) model (black), at the Pt$_{b_dual}$-O$_{b_vac}$ site on the surface and bulk co-doped Pt/In_2O_3(111) model (red).

Table S1. Calculated adsorption energies (E_{ad}, electronic energies only) of selected adsorbates from Eq. (3).

Species	E_{ad}/eV		
	O_{c_vac}	$Pt_{b\_surface}$-O_{b_vac}	Pt_{b_bulk}-O_{c_vac}
ln-CO_2	−0.21	−0.28	−0.20
bt-CO_2	1.15	−0.78	1.00
H_2	−0.06	−0.07	−0.05
CH_3OH	−0.66	−0.77	−0.49
CO	−0.15	−0.95	−0.16
H_2O	−0.65	−0.68	−0.65
H [a]	0.10	0.40	0.21

[a] E_{ad}(H) is calculated slightly differently as $E_{ad}(H) = E_{total} - (E_{slab} + \frac{1}{2} E_{H2})$.

Table S2. Calculated adhesive energies (ΔE_{adh}, electronic energies only) of a bulk-doped or surface-doped Pt atom with an In vacancy (V_{In}) in In_2O_3(111).

ΔE_{adh}(eV)	$Pt_{\_surface}$	$Pt_{\_bulk}$
In_a	-9.60	-9.70
In_b	-11.30	-10.76
In_c	-9.17	-9.04
In_d	-10.35	-9.35
In_e	-10.22	-9.68
In_f	-9.48	-10.32

Table S3. Calculated free formation energies of the surface V_O site on pristine In_2O_3(111), surface, and bulk doped Pt/In_2O_3(111) for H_2 reduction at 573 K.

$\Delta G_{f,VO}$(eV)	Pristine In_2O_3(111)	$Pt_{b\_surface}$	Pt_{b_bulk}
O_a	0.27	0.55	0.56
O_b	-0.59	-0.21	-0.06
O_c	-0.08	0.20	0.15
O_d	-0.44	0.31	0.10

Table S4. Relative energies (electronic energies only) for CO_2 hydrogenation to CH_3OH via the HCOO pathway.

Relative Energy (eV)	O_{c_vac}	$Pt_{b\_surface}$-O_{b_vac}	Pt_{b_bulk}-O_{c_vac}
***_D**	0.00	0.00	0.00
[ln-CO_2+H]*_D	0.25	-0.83	0.23
TS1	0.27	0.00	0.68
mono-HCOO*_D	-1.05	-0.14	-0.98
bi-HCOO*_D	-1.14	-0.91	-1.07
[HCOO+H]*_D	-0.05	0.07	-0.74
TS2	0.53	0.61	-0.05
H_2COO*_D	-0.76	-0.10	-0.80
TS3	-0.51	1.24	-0.65
[CH_2O-O]*_D	-0.67	-0.16	-0.65
[CH_2O+2H]*_P	-0.50	-0.66	-0.72
TS4	-0.20	0.29	-0.34
[CH_3O+H]*_P	-1.57	-2.27	-1.79
TS5	-1.42	0.22	-1.62
CH_3OH*_P	-1.44	-1.22	-2.01
***_D**	-0.66	-0.66	-0.66

Table S5. Relative energies (electronic energies only) for CO_2 direct dissociation to CO.

Relative Energy (eV)	O_{c_vac}	$Pt_{b\_surface}$-O_{b_vac}	Pt_b_bulk-O_{c_vac}
CO_2(g)+H_2(g)	0.00	0.00	0.00
bt-CO_2*+H_2(g)	1.15	-0.78	1.00
TS1	1.21	1.93	1.01
CO*+O*+H_2(g)	0.19	0.31	-0.04
O*+H_2(g)+ CO(g)	0.34	0.46	0.10
OH*+H*+CO(g)	0.32	-0.34	0.10
TS2	1.38	-0.04	1.26
H_2O*+CO(g)	0.05	-0.14	0.05
H_2O(g)+CO(g)	0.70	0.70	0.70

Table S6. Relative energies (electronic energies only) for CO_2 hydrogenation to CO via the COOH pathway.

Relative Energy (eV)	O_{c_vac}	$Pt_{b\_surface}$-O_{b_vac}	Pt_{b_bulk}-O_{c_vac}
$CO_2(g)+H_2(g)$	0.00	0.00	0.00
bt-CO_2*+H*+0.5H_2(g)	-0.50	-1.05	-1.12
TS1	0.53	0.68	1.09
COOH*+0.5H_2(g)	0.31	-0.46	0.80
TS2	0.32	-0.46	0.81
CO*+OH*+0.5H_2(g)	-0.58	-0.59	-0.54
OH*+0.5H_2(g)	-0.35	-0.36	-0.30
OH*+H*+CO(g)	0.32	-0.34	0.10
TS3	1.38	-0.04	1.26
H_2O*+CO(g)	0.05	-0.14	0.05
H_2O(g)+CO(g)	0.70	0.70	0.70

Table S7. Relative energies (electronic energies only) for CO hydrogenation to CH_3OH.

Relative Energy (eV)	O_{c_vac}	$Pt_{b\_surface}$-O_{b_vac}	Pt_{b_bulk}-O_{c_vac}
***_D**	0.00	0.00	0.00
[CO+H]*_D	0.34	-0.27	0.28
TS1	0.51	-0.21	0.81
[CHO+H]*_D	0.73	-1.20	0.51
TS2	0.81	-0.89	0.59
[CH_2O+H]*_D	-0.50	-1.02	-1.57
TS3	-0.44	-0.38	-0.34
[CH_3O+H]*_D	-1.77	-2.13	-2.00
TS4	-0.69	-0.76	-0.86
CH_3OH*_D	-2.02	-2.13	-1.85
***_D**	-1.36	-1.36	-1.36

Table S8. Elementary reactions considered in microkinetic simulations of CO_2 hydrogenation to methanol and CO on the In_2O_3(111) and Pt/In_2O_3(111) surfaces.
(“_s” and “_h” denote the V_O and “hydrogen reservoir” sites, respectively, “_g” indicates gaseous species, and “#” marks the beginning of a comment.)

Step	Elementary reaction
R1	CO2_g + *_s <-> CO2_s #ln-CO2
R2	CO2_g + *_s <-> O2C_s #bt-CO2
R3	CO2_s + H_h <-> [CO2-H_s] + *_h <-> HCOO_s + *_h
R4	HCOO_s + H_h <-> [HCOO-H_s] + *_h <-> H2COO_s + *_h
R5	H2COO_s <-> [H2CO-O_s] <-> OH2CO_s
R6	OH2CO_s + 2H_h <-> [OHH2CO-H_s] + 2*_h <-> OH3COH_s + 2*_h
R7	OH3COH_s <-> [OH3CO-H_s] <-> OCH3OH_s
R8	OCH3OH_s <-> CH3OH_g + O_s
R9	H2_g + 2*_h <-> [H-H_h] + *_h <-> 2H_h
R10	H2_g + O_s + *_h <-> [OH-H_s] + *_h <-> OH_s + H_h
R11	OH_s + H_h <-> [H-OH_s] + *_h <-> H2O_s + *_h
R12	H2O_s <-> H2O_g + *_s
R13	O_s + H_h <-> OH_s + *_h
R14	CO2_s + *_s <-> [CO-O_s] + *_s <-> CO_s + O_s
R15	CO_s <-> CO_g + *_s
R16	O2C_s + H_h <-> [O2C-H_s] + *_h <-> COOH_s + *_h
R17	COOH_s + *_s <-> [CO-OH_s] + *_s <-> CO_s + OH_s
R18	CO_s + H_h <-> [CO-H_s] + *_h <-> CHO_s + *_h
R19	CHO_s + H_h <-> [CHO-H_s] + *_h <-> OCH2_s + *_h
R20	OCH2_s + H_h <-> [CH2O-H_s] + *_h <-> OCH3_s + *_h
R21	OCH3_s + H_h <-> [CH3O-H_s] + *_h <-> CH3OH_s + *_h
R22	CH3OH_s <-> CH3OH_g + *_s

Table S9. Textural properties of various samples.

Sample	Measured Pt Loading[a] (wt.%)	Pt disperision[b] (%)	S_{BET}[c] ($m^2\ g^{-1}$)	V_{micro}[d] ($cm^3\ g^{-1}$)	V_{meso}[e] ($cm^3\ g^{-1}$)
In_2O_3	0	-	76	0.008	0.073
$1Pt/In_2O_3$	1.24	27.5	78	0.012	0.124
$3Pt/In_2O_3$	2.81	18.1	126	0.008	0.253
$1Pt/In_2O_3$-DI	1.37	-	46	0.002	0.115
$3Pt/In_2O_3$-DI	3.01	-	31	0.001	0.114

[a] Measured by ICP. [b] Obtained by CO chemisorption. [c] BET specific surface area. [d] Micropore volume determined by t-plot. [e] Mesopore volume determined by $V_{total}–V_{mico}$.

Table S10. Summary of catalysts for CO_2 hydrogenation to methanol.

Catalyst	H_2/CO_2 ratio	T (K)	p (MPa)	Space velocity (mL g_{cat}^{-1} h^{-1})	CO_2 conv. (%)	CH_3OH sel. (%)	STY (CH_3OH) (g g_{cat}^{-1} h^{-1})	SI Ref.
Ir/In_2O_3	4:1	573	5	21000	17.7	~70.0	0.765	
$Pd\text{-}P/In_2O_3$	4:1	573	5	21000	~20.0	~70.0	0.89	
$h\text{-}In_2O_3/Pd$	3:1	573	3	19200	~10.5	72.4	0.53	
Pt/In_2O_3	3:1	573	4	54000	5.7	~71.5	0.76	
	3:1	573	4	24000	~8.9	~66.5	~0.47	3
Ru/In_2O_3	4:1	573	5	21000	14.3	69.7	0.57	
Au/In_2O_3	4:1	573	5	21000	11.7	67.8	0.47	
Ni/In_2O_3	4:1	573	5	21000	18.4	~54.0	0.55	
In_2O_3@Co	4:1	523	5	15600	8.3	~87.0	0.65	
Rh/In_2O_3	4:1	573	5	45000	9.3	75	0.75	4
Co-RhIn/(5In5Al)O	3:1	543	4.5	36000	7.2	90.8	0.84	5
$Cu/3DZrO_x$	3:1	533	4.5	21,600	13.1	78.7	0.796	6
Cu-ZIF-8	3:1	533	4.5	21600	~22.0	~75.0	0.930	7
$1ZnO/Cu(OH)_2$	3:1	533	4.5	37600	15.2	51.1	0.996	8
$3ZnO/Cu(OH)_2$	3:1	533	4.5	21600	21.9	56.0	0.958	
F-CuZn_553	3:1	493	4.0	56571	1.9	82.3	0.656	9
$Cu/ZnO/Al_2O_3$	3:1	533	1.5	60000	-	48	0.538	10
$Inverse\text{-}ZrO_2/Cu$	3:1	493	3	48000	<5	~70	0.524	11
$ZnO\text{-}ZrO_2$	3:1	593	5	24000	10	91	0.720	12
$Ga/Zn/ZrO_x$	3:1	593	5	24000	8.8	87.4	0.630	13
In_2O_3/ZrO_2	4:1	573	5	20000	5.2	99.8	0.321	14
$PdZn/ZnO/SiO_2$	3:1	533	5.0	-	3.6	65.3	0.443	15

Catalyst	H_2/CO_2 ratio	*T* (K)	*p* (MPa)	Space velocity (mL g_{cat}^{-1} h^{-1})	CO_2 conv. (%)	CH_3OH sel. (%)	STY (CH_3OH) (g g_{cat}^{-1} h^{-1})	SI Ref.
$PdZn/ZnO/ZnFe_2O_4$	3:1	563	5.0	21600	13.94	55.02	0.593	16
Pd@ZIF-8	3:1	543	4.5	-	15	56.2	0.65	17
$InNi_3C_{0.5}/Fe_3O_4$	3:1	573	4	24000	8.9	91.4	0.71	18
$Ni_3InC_{0.5}$/monoclinic-ZrO_2	3:1	573	5	24000	8.5	87.9	0.62	
MoS_2	3:1	453	5	3000	12.5	94.3	0.13	19
$1Pt/In_2O_3$	3:1	573	5	36000	10.4	76.1	0.98	This work
				45000	8.2	81.6	1.03	
				54000	7.7	84.8	1.25	
$3Pt/In_2O_3$	3:1	553	5	36000	11.7	78.0	1.13	
				45000	10.3	78.5	1.25	
				54000	8.4	76.1	1.18	

Table S11. EXAFS fitting parameters at the Pt L_3-edge for various samples (S_0^2 = 0.84).

Sample	Condition	Shell	CN[a]	R[b] (Å)	σ^{2c}	ΔE_0[d]	R factor[e]
Pt Foil		Pt-Pt	12*	2.76±0.01	0.0047	7.2±0.3	0.0023
PtO_2		Pt-O	6*	2.02±0.01	0.0028	8.1±0.1	0.0067
1Pt/In_2O_3	Ar	Pt-O	4.7±0.2	2.02±0.02	0.0032	13.9±0.9	0.0104
3Pt/In_2O_3		Pt-O	4.4±0.3	2.01±0.02	0.0031	12.5±1.7	0.0119
1Pt/In_2O_3-DI		Pt-O	4.1±0.1	2.00±0.02	0.0042	12.1±1.2	0.0175
3Pt/In_2O_3-DI		Pt-O	3.8±0.1	2.00±0.03	0.0045	10.9±1.3	0.0123
1Pt/In_2O_3	1 h	Pt-O	2.6±0.2	2.06±0.01	0.0031	18.1±0.7	0.0102
3Pt/In_2O_3		Pt-O	2.4±0.1	2.04±0.01	0.0042	16.5±1.0	0.0099
1Pt/In_2O_3-DI		Pt-O	1.7±0.2	2.11±0.02	0.0079	20.5±1.5	0.0123
		Pt-In	1.2±0.2	2.81±0.01	0.0055		
		Pt-Pt	2.0±0.7	3.26±0.03	0.0031		
3Pt/In_2O_3-DI		Pt-In	5.9±0.2	2.74±0.01	0.0076	7.9±0.7	0.0040
		Pt-Pt	5.9±1.3	2.83±0.02	0.0092		
1Pt/In_2O_3	48 h	Pt-O	2.4±0.2	2.09±0.02	0.0038	19.2±1.2	0.0157
3Pt/In_2O_3		Pt-O	2.3±0.1	2.07±0.01	0.0058	17.8±1.4	0.0132
1Pt/In_2O_3-DI		Pt-O	1.5±0.2	2.10±0.03	0.0053	20.7±1.6	0.0187
		Pt-In	2.0±0.3	2.81±0.01	0.0069		
		Pt-Pt	3.4±1.0	3.29±0.03	0.0046		
3Pt/In_2O_3-DI		Pt-In	5.5±0.3	2.74±0.01	0.0052	9.0±1.1	0.0143
		Pt-Pt	6.3±2.5	2.84±0.03	0.0048		

[a] CN = coordination numbers; [b] R = bond distance; [c] σ^2 = Debye-Waller factors; [d] ΔE_0 = inner potential correction. [e] R factor = goodness of fit.

Table S12. Deconvolution results of Pt $4d_{5/2}$ XPS peaks.

Situation	Sample	Atomic content (%)		
		Red Pt^{4+} /317.0 eV	Blue Pt^{2+} /315.3eV	Yellow Pt^{0} /314.2 eV
fresh	1Pt/In_2O_3	50.67	49.33	0
	3Pt/In_2O_3	54.86	45.14	0
	1Pt/In_2O_3-DI	100	0	0
	3Pt/In_2O_3-DI	100	0	0
Ar	1Pt/In_2O_3	39.94	60.06	0
	3Pt/In_2O_3	72.85	27.15	0
	1Pt/In_2O_3-DI	100	0	0
	3Pt/In_2O_3-DI	100	0	0
1 h	1Pt/In_2O_3	0	100	0
	3Pt/In_2O_3	0	100	0
	1Pt/In_2O_3-DI	31.97	0	68.03
	3Pt/In_2O_3-DI	37.44	0	62.56
48 h	1Pt/In_2O_3	0	100	0
	3Pt/In_2O_3	0	100	0
	1Pt/In_2O_3-DI	34.41	0	68.59
	3Pt/In_2O_3-DI	40.13	0	59.87

Table S13. Quantification of CO_2 chemisorbed on the catalysts.

Pretreatment conditions[a]	In_2O_3	$1Pt/In_2O_3$	$3Pt/In_2O_3$	$1Pt/In_2O_3$-DI	$3Pt/In_2O_3$-DI
Ar[b]	3.57	7.41	11.58	9.37	2.66
H_2[b]	3.08	3.91	2.04	3.18	2.43

[a] All samples were pretreated in Ar or H_2 at 573 K for 1 h. [b] mmol g_{cat}^{-1}.

Table S14. Calculated Bader charges and the formal oxidation states of the Pt single atom sites. Numbers in the paratheses are estimated from the linear relationship shown in Figure S13b.

	Bader charge (|e|)	Formal oxidation state
Pt	0.00	0
Pt_2O	0.43	+1
PtO	0.98	+2
Pt_3O_4	1.12	+2.67
PtO_2	1.49	+3
$Pt_{b\_surface}$	1.40	(+3.5)
$Pt_{b\_surface}$-O_{b_vac}	0.81	(+1.9)
Pt_{b_bulk}	1.39	(+3.5)
Pt_{b_bulk}-O_{c_vac}	1.39	(+3.5)

Table S15. Calculated rate constants of elementary steps for the $In_2O_3(111)$, $Pt_{b\text{-surface}}$ and $Pt_{b\text{-bulk}}$ models at 573 K. All the rate constants were calculated based on the transition state theory as implemented in CatMAP. Only the rate constants of the forward direction are listed, although those for both directions were calculated in the microkinetic simulations.

Step	Elementary reaction	Rate constant		
		O_{c_vac}	$Pt_{b\_surface}$-O_{b_vac}	Pt_{b_bulk}-O_{c_vac}
R1	CO2_g+s->CO2_s	3.68E+04	3.57E+09	3.02E+04
R2	CO2_g+s->O2C_s	2.51E-05	2.30E+11	3.26E-04
R3	CO2_s+H_t->[CO2-H_s]+t->HCOO_s+t	9.68E+12	1.86E+03	2.81E+10
R4	HCOO_s+H_t->[HCOO-H_s]+t->H2COO_s+t	1.97E-01	2.39E-01	5.74E+05
R5	H2COO_s->[H2CO-O_s] ->OH2CO_s	4.42E+11	2.45E+02	2.96E+12
R6	OH2CO_s+H_t+H_t->[OHH2CO-H_s]+2t->OH3COH_s+2t	3.83E+06	6.30E-06	1.19E+13
R7	OH3COH_s->[OH3CO-H_s] ->OCH3OH_s	4.43E+12	4.84E-10	3.60E+11
R8	OCH3OH_s->CH3OH_g+O_s	1.19E+13	1.19E+13	1.19E+13
R9	H2_g+t+t->[H-H_t]+t->H_t+H_t	1.68E+05	1.19E+13	2.04E+03
R10	H2_g+O_s+t->[OH-H_s]+t->OH_s+H_t	2.96E-01	3.86E-11	1.57E-01
R11	OH_s+H_t->[H-OH_s]+t->H2O_s+t	1.26E-01	1.30E+05	3.04E+01
R12	H2O_s->H2O_g+s	1.19E+13	1.19E+13	1.19E+13
R13	O_s+H_t->OH_s+t	1.19E+13	1.19E+13	1.19E+13
R14	CO2_s + s -> [CO-O_s] + s -> CO_s + O_s	/	3.97E-09	1.92E+04
R15	CO_s->CO_g+s	1.19E+13	1.19E+13	1.19E+13
R16	O2C_s+H_t->O2C-H_s+t->COOH_s+t	1.19E+13	/	1.19E+13
R17	COOH_s+s->CO-OH_s+s->CO_s+OH_s	1.12E+12	/	4.56E+10
R18	CO_s+H_t->CO-H_s+t->CHO_s+t	4.85E+09	7.17E+01	2.49E+07
R19	CHO_s+H_t->CHO-H_s+t->OCH2_s+t	2.17E+09	3.86E+02	2.25E+12
R20	OCH2_s+H_t->CH2O-H_s+t->OCH3_s+t	1.19E+13	1.40E-07	8.05E+08
R21	OCH3_s+H_t->CH3O-H_s+t->CH3OH_s+t	4.46E-02	7.96E-08	5.30E+01
R22	CH3OH_s->CH3OH_g+s	1.19E+13	1.19E+13	1.19E+13

Table S16. Calculated energy barriers (E_a) and reaction energies (E_r) for H migration for the In_2O_3(111), $Pt_{b\_surface}$, and Pt_{b_bulk} models.

Structure	Pathway	E_a/eV	E_r/eV
In_2O_3(111)	In8→O4	1.18	-0.73
	In8→In11	0.34	0.33
In_2O_3(111) with a secondary H on In4	In8→O4	1.28	-1.05
	In8→In11	0.14	0.13
$Pt_{b\_surface}$	Pt6→O2	1.11	-0.45
	Pt6→In10	1.15	1.00
$Pt_{b\_surface}$ with a secondary H on In3	Pt6→O2	1.05	-0.71
	Pt6→In10	1.27	1.24
Pt_{b_bulk}	In8→O4	1.14	-0.62
	In8→In11	0.26	0.21
Pt_{b_bulk} with a secondary H on In4	In8→O4	1.26	-0.82
	In8→In11	0.20	0.20

Supplementary References.

S1. G. Henkelman, A. Arnaldsson and H. Jónsson, *Comput Mater Sci*, 2006, **36**, 354-360.

S2. E. Sanville, S. D. Kenny, R. Smith and G. Henkelman, *J Comput Chem*, 2007, **28**, 899-908.

S3. D. Cai, Y. Cai, K. B. Tan and G. Zhan, *Materials*, 2023, **16**, 2803.

S4. S. N. H. Dostagir, C. B. Thompson, H. Kobayashi, A. M. Karim and A. Shrotri, *Catal. Sci. Technol.*, 2021, **10**, 8196-8202.

S5. M. M. J. Li, H. Zou, J. Zheng, T. S. Wu, T. S. Chan, Y. L. Soo, X. P. Wu, X. Q. Gong, T. Chen, K. Roy, G. Held and S. C. E. Tsang, *Angew. Chem. Int. Ed.*, 2020, **59**, 16039-16046.

S6. T. Liu, X. Hong and G. Liu, *ACS Catalysis*, 2020, **10**, 93-102.

S7. B. Hu, Y. Yin, Z. Zhong, D. Wu, G. Liu and X. Hong, *Catal Sci Technol*, 2019, **9**, 2673-2681.

S8. X. Liu, J. Luo, H. Wang, L. Huang, S. Wang, S. Li, Z. Sun, F. Sun, Z. Jiang and S. Wei, *Angew. Chem. Int. Ed.*, 2022, **61**, e202202330.

S9. V. Dybbert, S. M. Fehr, F. Klein, A. Schaadt, A. Hoffmann, E. Frei, E. Erdem, T. Ludwig, H. Hillebrecht and I. Krossing, *Angew. Chem. Int. Ed.*, 2019, **58**, 12935-12939.

S10. M. Zabilskiy, V. L. Sushkevich, M. A. Newton and J. A. Van Bokhoven, *ACS Catal.*, 2020, **10**, 14240-14244.

S11. C. Wu, L. Lin, J. Liu, J. Zhang and D. Ma, *Nat. Commun.*, 2020, **11**, 5767.

S12. J. Wang, G. Li, Z. Li, C. Tang, Z. Feng, H. An, H. Liu, T. Liu and C. Li, *Sci. Adv.*, 2017, **3**, e1701290.

S13. F. Sha, C. Tang, S. Tang, Q. Wang, Z. Han, J. Wang and C. Li, *J. Catal.*, 2021, **404**, 383-392.

S14. O. Martin, A. J. Martín, C. Mondelli, S. Mitchell, T. F. Segawa, R. Hauert, C. Drouilly, D. Curulla-Ferré and J. Pérez-Ramírez, *Angew. Chem. Int. Ed.*, 2016, **55**, 6261-6265.

S15. M. Zabilskiy, V. L. Sushkevich, M. A. Newton, F. Krumeich, M. Nachtegaal and J. A. Bokhoven, *Angew. Chem. Int. Ed.*, 2021, **60**, 17053-17059.

S16. Y. Wang, D. Wu, T. Liu, G. Liu and X. Hong, *Journal of colloid and interface science*, 2021, **597**, 260-268.

S17. Y. Yin, X. Bing, X. Zhou, X. Hong and G. Liu, *Appl. Catal. B: Environ.*, 2018, **234**, 143-152.

S18. C. Meng, G. Zhao, X. R. Shi, P. Chen, Y. Liu and Y. Lu, *Sci. Adv.*, 2021, **7**, abi6012.

S19. J. Hu, L. Yu, J. Deng, Y. Wang, K. Cheng, C. Ma, Q. Zhang, W. Wen, S. Yu, Y. Pan, J. Yang, H. Ma, F. Qi, Y. Wang, Y. Zheng, M. Chen, R. Huang, S. Zhang, Z. Zhao, J. Mao, X. Meng, Q. Ji, G. Hou, X. Han, X. Bao, Y. Wang and D. Deng, *Nat. Catal.*, 2021, **4**, 242-250.

Optimized coordinates.

The structure of O_{c_vac} site on the pristine In_2O_3(111) model.

```
In    O
   1.00000000000000
     7.2221500012007906   -12.5091307391902902     0.0000000000000060
     0.0000000000000000     8.3394204937178671   -11.7937215635675585
    14.6850992550548085     8.4784460098618144     5.9951666679957052
   In    O
    48    71
Selective dynamics
Direct
  0.8515836378845805  0.4089291826345161  0.3472970745831390   F   F   F
  0.5150245914900321  0.7440169721361686  0.5107315124964786   T   T   T
  0.1787936890341729  0.0787346890256027  0.6841346174597788   T   T   T
  0.8291001228075459  0.9356178259191950  0.3251822334614900   F   F   F
  0.4951056047961073  0.2660620800789640  0.4968343422877485   T   T   T
  0.1609281290305564  0.6026696688509230  0.6619426644787515   T   T   T
  0.3248949945999087  0.4314126977115507  0.3251822334614900   F   F   F
  0.9940745370838551  0.7646081243098523  0.4940448122225525   T   T   T
  0.6597502785703476  0.1001724195076380  0.6726034020991035   T   T   T
  0.8403418803460667  0.6722735042768520  0.3362396540223145   F   F   F
  0.5069863334583480  0.0070607263158987  0.5048350010116757   T   T   T
  0.1687909624471381  0.3292651525912543  0.6717497474286122   T   T   T
  0.1065177031116420  0.6835152618153728  0.3251822334614900   F   F   F
  0.7765179567201185  0.0145515363917361  0.4941065213529806   T   T   T
  0.4489350411563409  0.3467701301946983  0.6650858960867200   T   T   T
  0.5994810737807654  0.4426544552500715  0.3472970745831390   F   F   F
  0.2672742569735468  0.7772087686617817  0.5107834234786717   T   T   T
  0.9262410723333766  0.1033066863801731  0.6847315499916394   T   T   T
  0.0952759455731211  0.4426544552500715  0.3472970745831461   F   F   F
  0.7644220695978731  0.7734449049399712  0.5167335888994488   T   T   T
  0.4356459748316076  0.1168513267089597  0.6799527934028261   T   T   T
  0.0727924304960865  0.9018925533036395  0.3251822334614900   F   F   F
  0.7428000944078721  0.2308768497348092  0.4990481937607448   T   T   T
  0.4048884566139211  0.5679185646650453  0.6572928951825260   T   T   T
  0.5657558011652100  0.6610317467383382  0.3472970745831461   F   F   F
  0.2337817565971952  0.9939317528785960  0.5177637265267626   T   T   T
  0.8934830693472149  0.3235448895875112  0.6795026573279173   T   T   T
  0.8403418803460667  0.1680683760692148  0.3362396540223145   F   F   F
  0.5004101948575349  0.5016592518854255  0.5035359433096305   T   T   T
```

0.1627270417983703	0.8342711708057631	0.6716874440926097	T	T	T
0.5657558011652100	0.1568266185306939	0.3472970745831461	F	F	F
0.2303086252596035	0.4927466367354448	0.5078905634472353	T	T	T
0.9023627123224102	0.8262623374393062	0.6847387182803629	T	T	T
0.1065177031116420	0.1793101336077285	0.3251822334614900	F	F	F
0.7772491466085952	0.5138815911219601	0.4985206630978367	T	T	T
0.4501589012784232	0.8542262188473980	0.6575851634290834	T	T	T
0.5769975587037308	0.9018925533036395	0.3251822334614900	F	F	F
0.2432383032407795	0.2320333454446220	0.4933615954135943	T	T	T
0.9106868453355121	0.5651144394095267	0.6714502988276043	T	T	T
0.3473785096769433	0.9131343108421603	0.3472970745831461	F	F	F
0.0138376428887941	0.2431727126854084	0.5169835304258714	T	T	T
0.6849302066422637	0.5732946563351607	0.6808446045427993	T	T	T
0.3361367521384224	0.1680683760692148	0.3362396540223145	F	F	F
0.0033770545345658	0.5051697636669557	0.5060035213766770	T	T	T
0.6768030556099109	0.8474735337364911	0.6695896307206323	T	T	T
0.3361367521384295	0.6722735042768520	0.3362396540223145	F	F	F
0.0036652155240213	0.0030790942370231	0.5053037215688507	T	T	T
0.6733184446655325	0.3378837004516030	0.6892271898344912	T	T	T
0.2541842590098113	0.7461778751490158	0.3944775844339503	F	F	F
0.9219585109919451	0.0763691388351082	0.5653024490432083	T	T	T
0.5934260847573514	0.4212218337260384	0.7329353977136296	T	T	T
0.0094723336752622	0.5311979178146160	0.3799386832336822	F	F	F
0.6779418337985288	0.8622514581196958	0.5485523800133172	T	T	T
0.3409608775750058	0.1963777071944381	0.7124834817538314	T	T	T
0.9439217482440156	0.1009536314534927	0.3071906159917361	F	F	F
0.6082322100826510	0.4375541352971201	0.4732454235560060	T	T	T
0.2828910732287889	0.7764270484885394	0.6605957001130667	T	T	T
0.9074566249617817	0.8429681167905230	0.3071906159917361	F	F	F
0.5737727706559108	0.1773115212829676	0.4725798537518203	T	T	T
0.2382301633862800	0.5077804435623474	0.6786697061009932	T	T	T
0.5217255841393538	0.9989379227400192	0.3799386832336822	F	F	F
0.1924124688276860	0.3345454404764561	0.5504111727139035	T	T	T
0.8507686881784088	0.6660902132057623	0.7164521320317504	T	T	T
0.4100411230105863	0.8281303682776340	0.2780017236106858	F	F	F
0.0786825443748833	0.1605930244925457	0.4474704766076409	T	T	T
0.7468023358114139	0.4895979579332608	0.6150985090328221	T	T	T
0.3978860819165106	0.0618058007524454	0.3019131806672561	F	F	F
0.0624059583030114	0.3997740824850230	0.4716123327359488	T	T	T
0.7227001922801661	0.7287891470277142	0.6399218666303513	T	T	T
0.0083537854409172	0.7340228340549402	0.3705661273773728	F	F	F

0.6708961109158443	0.0637814748358349	0.5389424342999040	T	T	T
0.7367620124481107	0.2351831206849297	0.3652886920528999	F	F	F
0.3962972292018760	0.5729841984975722	0.5361837208325596	T	T	T
0.0718421419396710	0.9105867137804338	0.7080114423922272	T	T	T
0.6723299752512091	0.6105241744987708	0.3019131806672561	F	F	F
0.3410617496276204	0.9462980970793158	0.4724995739456053	T	T	T
0.0074805172945991	0.2790500209266236	0.6379556782342228	T	T	T
0.7340793050292973	0.0000564709743571	0.3705661273773728	F	F	F
0.3984638853439720	0.3381976318329443	0.5398826723149766	T	T	T
0.0724725152722380	0.6732473843099857	0.7055053012239978	T	T	T
0.4919936161392044	0.7542259974054701	0.3944775844339503	F	F	F
0.1600420928560443	0.0861499552678247	0.5649144440537728	T	T	T
0.8340885098648426	0.4153846610320791	0.7339672499800191	T	T	T
0.5068313646520934	0.2716482439671637	0.3652886920528999	F	F	F
0.1818090783263110	0.6091205027011165	0.5395560644075044	T	T	T
0.8414385448085455	0.9335380816177623	0.7080050764773403	T	T	T
0.1654421396247585	0.0644885081712587	0.3071906159917361	F	F	F
0.8324923253709929	0.3986177272367389	0.4735348723426871	T	T	T
0.5014687899139016	0.7331192243347868	0.6528180314401207	T	T	T
0.9466044556628361	0.3360802811640724	0.3019131806672561	F	F	F
0.6066866150627402	0.6666407514980031	0.4729082292862552	T	T	T
0.2758894594743814	0.0004594315708638	0.6436200545031867	T	T	T
0.6628011706015897	0.8133490907390950	0.2925406248109539	F	F	F
0.3301758797286338	0.1457918890908664	0.4599969012245183	T	T	T
0.9982096511810418	0.4777212779586466	0.6270455588382918	T	T	T
0.2622323812662657	0.5164166402760770	0.3944775844339503	F	F	F
0.9292380778480052	0.8467164462469423	0.5654475902923017	T	T	T
0.5855467475252533	0.1769396102648887	0.7352914834108233	T	T	T
0.4772123386006655	0.4866846722759277	0.3799386832336822	F	F	F
0.1475065113728523	0.8188437496726967	0.5503252227382736	T	T	T
0.8200223512156932	0.1577592223413984	0.7167951917447803	T	T	T
0.4180892452670406	0.5983691334046952	0.2780017236106858	F	F	F
0.0853687396340789	0.9292064000746429	0.4478923319747615	T	T	T
0.7461846751705845	0.2605544269072839	0.6156804082185114	T	T	T
0.2743874223603413	0.2743309513859842	0.3705661273773728	F	F	F
0.9449357327045759	0.6101750463974757	0.5401951488901106	T	T	T
0.6062185442790496	0.9381922927583286	0.7053719269961032	T	T	T
0.1802798881376475	0.5903210111482409	0.2780017236106858	F	F	F
0.8490147139634594	0.9219008840428325	0.4464726329729786	T	T	T
0.5216745337018605	0.2613341189766154	0.6132303782822828	T	T	T
0.1505479201374982	0.3456090858136918	0.2925406248109539	F	F	F

0.8208755977275422	0.6781803301803920	0.4592838137657662	T	T	T
0.4882759856501566	0.0165205651580170	0.6257110292124958	T	T	T
0.1950611656761865	0.8578623362777833	0.2925406248109539	F	F	F
0.8636133802325497	0.1869981506035004	0.4589154456272324	T	T	T
0.5164107875499319	0.5148746884662944	0.6331353107191199	T	T	T
0.7732271357303446	0.5015788917631880	0.3652886920528999	F	F	F
0.4366308514393248	0.8329093074368344	0.5355443883260358	T	T	T
0.0947771110450634	0.1633385920726788	0.7099764018096762	T	T	T

The structure of $Pt_{b\_surface}$-O_{b_vac} site on the surface-doped Pt/In_2O_3(111) model.

```
In Pt    O
   1.00000000000000
     7.2221500012007906   -12.5091307391902902     0.0000000000000060
     0.0000000000000000     8.3394204937178671   -11.7937215635675585
    14.6850992550548085     8.4784460098618144     5.9951666679957052
   In     Pt     O
    47      1     71
Selective dynamics
Direct
  0.8515836378845805  0.4089291826345161  0.3472970745831390   F   F   F
  0.5144163451068643  0.7420627182455818  0.5103230663870764   T   T   T
  0.1780429720699312  0.0782018489444792  0.6851963085930772   T   T   T
  0.8291001228075459  0.9356178259191950  0.3251822334614900   F   F   F
  0.4959056253475813  0.2671136676372907  0.4962358394770599   T   T   T
  0.1592789516668620  0.6048668015193429  0.6591309994981019   T   T   T
  0.3248949945999087  0.4314126977115507  0.3251822334614900   F   F   F
  0.9944931349326480  0.7646160347119347  0.4939830940513519   T   T   T
  0.6630093588801829  0.1028843251231923  0.6691060532097628   T   T   T
  0.8403418803460667  0.6722735042768520  0.3362396540223145   F   F   F
  0.5058053490121125  0.0051167955023209  0.5050539865750020   T   T   T
  0.1700960622901754  0.3323419473343198  0.6706510439230949   T   T   T
  0.1065177031116420  0.6835152618153728  0.3251822334614900   F   F   F
  0.7762775580587139  0.0133518373716017  0.4938198717150047   T   T   T
  0.4254653946804459  0.3403589866719128  0.6604060757945430   T   T   T
  0.5994810737807654  0.4426544552500715  0.3472970745831390   F   F   F
  0.2663864537118484  0.7770650040002861  0.5100645256245612   T   T   T
  0.9274357113406366  0.1055923206471549  0.6860545369698122   T   T   T
  0.0952759455731211  0.4426544552500715  0.3472970745831461   F   F   F
  0.7656980518926559  0.7749139639718148  0.5161047177798238   T   T   T
  0.4380271437628180  0.1200335384807808  0.6794965001425133   T   T   T
  0.0727924304960865  0.9018925533036395  0.3251822334614900   F   F   F
  0.7434647416251251  0.2280704700343665  0.4944516969456175   T   T   T
  0.4040903739898303  0.5606076059625331  0.6612047922901757   T   T   T
  0.5657558011652100  0.6610317467383382  0.3472970745831461   F   F   F
  0.2339628087770320  0.9941668206897645  0.5182023389123017   T   T   T
  0.8896192362506908  0.3222485939701059  0.6800453347169302   T   T   T
  0.8403418803460667  0.1680683760692148  0.3362396540223145   F   F   F
  0.5033936062462513  0.5024518982535404  0.5030671772362795   T   T   T
  0.1641263929526402  0.8353705153617130  0.6718273782385559   T   T   T
  0.5657558011652100  0.1568266185306939  0.3472970745831461   F   F   F
```

0.2315118870982441	0.4939470433690535	0.5106511281490932	T	T	T
0.9041314568524513	0.8297066906054045	0.6846708700019517	T	T	T
0.1065177031116420	0.1793101336077285	0.3251822334614900	F	F	F
0.7780536311955716	0.5129560602801641	0.4956726287178961	T	T	T
0.4499655987505083	0.8518174347063420	0.6589838948894829	T	T	T
0.5769975587037308	0.9018925533036395	0.3251822334614900	F	F	F
0.2414460985867522	0.2313532263192414	0.4919607183361330	T	T	T
0.9106098219798667	0.5647069848680675	0.6703374171928879	T	T	T
0.3473785096769433	0.9131343108421603	0.3472970745831461	F	F	F
0.0136382217091421	0.2434094773385411	0.5178974908450326	T	T	T
0.6908771409771540	0.5784058745456029	0.6757877193524910	T	T	T
0.3361367521384224	0.1680683760692148	0.3362396540223145	F	F	F
0.0023287728414916	0.5038929113398355	0.5059152349786529	T	T	T
0.6767990242216968	0.8472878289079384	0.6701296348312589	T	T	T
0.3361367521384295	0.6722735042768520	0.3362396540223145	F	F	F
0.0044441779200839	0.0038850973832904	0.5060174382320658	T	T	T
0.6684856226187866	0.3440988355575483	0.6735611983237193	T	T	T
0.2541842590098113	0.7461778751490158	0.3944775844339503	F	F	F
0.9215131005983579	0.0767326739149771	0.5663631047559983	T	T	T
0.0094723336752622	0.5311979178146160	0.3799386832336822	F	F	F
0.6756351915361520	0.8604029773630290	0.5490634984344334	T	T	T
0.3410407149092538	0.1898068342848915	0.7150315351502363	T	T	T
0.9439217482440156	0.1009536314534927	0.3071906159917361	F	F	F
0.6088001177229758	0.4374713599149443	0.4734794942040625	T	T	T
0.2828571806819339	0.7768320751954374	0.6627679041252605	T	T	T
0.9074566249617817	0.8429681167905230	0.3071906159917361	F	F	F
0.5723754420051761	0.1767388221939826	0.4742499052087940	T	T	T
0.2327302576278528	0.5112530494417888	0.6605805038359217	T	T	T
0.5217255841393538	0.9989379227400192	0.3799386832336822	F	F	F
0.1907279595118423	0.3324997128218064	0.5495065560314267	T	T	T
0.8507383102790524	0.6664836756461948	0.7159800584868222	T	T	T
0.4100411230105863	0.8281303682776340	0.2780017236106858	F	F	F
0.0774989509290452	0.1594568304992410	0.4473360864943011	T	T	T
0.7454178435400859	0.4886441617849516	0.6142962090061371	T	T	T
0.3978860819165106	0.0618058007524454	0.3019131806672561	F	F	F
0.0629022000317264	0.4000267545418107	0.4726813268170205	T	T	T
0.7273949755104676	0.7336046107601746	0.6382217329812582	T	T	T
0.0083537854409172	0.7340228340549402	0.3705661273773728	F	F	F
0.6673911839520204	0.0585496136211405	0.5355267106500831	T	T	T
0.3313743210242923	0.4020947301668266	0.7054560586979789	T	T	T
0.7367620124481107	0.2351831206849297	0.3652886920528999	F	F	F

0.4005753555857676	0.5704790642454671	0.5391318737254169	T	T	T
0.0726701945552358	0.9107817367903627	0.7097707000348553	T	T	T
0.6723299752512091	0.6105241744987708	0.3019131806672561	F	F	F
0.3411513765631272	0.9456759715238078	0.4730905932352471	T	T	T
0.0082085407848061	0.2805905766771544	0.6401016957411624	T	T	T
0.7340793050292973	0.0000564709743571	0.3705661273773728	F	F	F
0.3970927309682556	0.3389781786630318	0.5381564226522181	T	T	T
0.0714372561953384	0.6739291480835531	0.7059269680527704	T	T	T
0.4919936161392044	0.7542259974054701	0.3944775844339503	F	F	F
0.1609095900864847	0.0872817236849406	0.5657348241531807	T	T	T
0.8142989863087684	0.4094897288685947	0.7263785500168290	T	T	T
0.5068313646520934	0.2716482439671637	0.3652886920528999	F	F	F
0.1782228163587360	0.6100837841055375	0.5372224594197658	T	T	T
0.8420285372294464	0.9349918657064245	0.7093584845492301	T	T	T
0.1654421396247585	0.0644885081712587	0.3071906159917361	F	F	F
0.8326891832508710	0.3985728155154050	0.4729874070701329	T	T	T
0.4993224098116187	0.7269272065393854	0.6619564704558234	T	T	T
0.9466044556628361	0.3360802811640724	0.3019131806672561	F	F	F
0.6079988928477075	0.6668279692257679	0.4726988851670414	T	T	T
0.2766530185401472	0.0001669814434895	0.6419583539804924	T	T	T
0.6628011706015897	0.8133490907390950	0.2925406248109539	F	F	F
0.3308618482303172	0.1463685225774713	0.4609115997294877	T	T	T
0.9950668229791066	0.4776593743249350	0.6293476243849752	T	T	T
0.2622323812662657	0.5164166402760770	0.3944775844339503	F	F	F
0.9313788610647881	0.8478680269105111	0.5657103172763452	T	T	T
0.5975083879763882	0.1973971880564440	0.7262396162358885	T	T	T
0.4772123386006655	0.4866846722759277	0.3799386832336822	F	F	F
0.1469159054587232	0.8180124804821908	0.5506973452398446	T	T	T
0.8208993091276284	0.1585237181265251	0.7214300745417720	T	T	T
0.4180892452670406	0.5983691334046952	0.2780017236106858	F	F	F
0.0861635317216290	0.9297539720485278	0.4482402333398083	T	T	T
0.7567766136651739	0.2518514654818088	0.6084260724239671	T	T	T
0.2743874223603413	0.2743309513859842	0.3705661273773728	F	F	F
0.9427940983496370	0.6089864710737525	0.5413350699277326	T	T	T
0.6074032178705331	0.9396920813144303	0.7036200158724121	T	T	T
0.1802798881376475	0.5903210111482409	0.2780017236106858	F	F	F
0.8494066210340212	0.9220583418686458	0.4470886117026101	T	T	T
0.5210719631606825	0.2730055785314461	0.6168176700320059	T	T	T
0.1505479201374982	0.3456090858136918	0.2925406248109539	F	F	F
0.8212394512957965	0.6782460349075130	0.4598626968572128	T	T	T
0.4893414748203754	0.0174143057790597	0.6279797698912470	T	T	T

0.1950611656761865	0.8578623362777833	0.2925406248109539	F	F	F
0.8649873692190474	0.1853557042356371	0.4578768723348168	T	T	T
0.5316649115128755	0.5116804393570299	0.6374434910292263	T	T	T
0.7732271357303446	0.5015788917631880	0.3652886920528999	F	F	F
0.4348059011948170	0.8291680002457963	0.5377716836417862	T	T	T
0.0962710359487064	0.1655116270560691	0.7088954979694451	T	T	T

The structure of Pt_{b_bulk}-O_{c_vac} site on the bulk-doped Pt/In_2O_3(111) model.

```
In Pt In    O
   1.00000000000000
     7.2221500012007906   -12.5091307391902902     0.0000000000000060
     0.0000000000000000     8.3394204937178671   -11.7937215635675585
    14.6850992550548085     8.4784460098618144     5.9951666679957052
   In    Pt    In    O
    46     1     1    71
Selective dynamics
Direct
  0.8515836378845805  0.4089291826345161  0.3472970745831390   F   F   F
  0.5140644324236991  0.7427620229964087  0.5105878300073140   T   T   T
  0.1766902928655739  0.0764841071297987  0.6836994673266034   T   T   T
  0.8291001228075459  0.9356178259191950  0.3251822334614900   F   F   F
  0.4956303587476827  0.2666788646373073  0.4966492216034552   T   T   T
  0.1601430720508848  0.6026358488075120  0.6605764215066546   T   T   T
  0.3248949945999087  0.4314126977115507  0.3251822334614900   F   F   F
  0.9924621731904772  0.7636886773674421  0.4929885845740931   T   T   T
  0.6591507019240208  0.0997335346358127  0.6711746948231420   T   T   T
  0.8403418803460667  0.6722735042768520  0.3362396540223145   F   F   F
  0.5068833895094028  0.0067773254202166  0.5042432214488231   T   T   T
  0.1772055381113772  0.3307079818001839  0.6716740851170948   T   T   T
  0.1065177031116420  0.6835152618153728  0.3251822334614900   F   F   F
  0.7774052027323788  0.0164978972382845  0.4935343558128613   T   T   T
  0.4475395178335740  0.3480080632484079  0.6653635640131571   T   T   T
  0.5994810737807654  0.4426544552500715  0.3472970745831390   F   F   F
  0.2672110537485038  0.7770364483461150  0.5104088586011829   T   T   T
  0.9299512039023639  0.1039819740945987  0.6846522119789811   T   T   T
  0.0952759455731211  0.4426544552500715  0.3472970745831461   F   F   F
  0.7639394689456689  0.7744519613352346  0.5161754974917153   T   T   T
  0.4351634726148905  0.1172431446641152  0.6783617721440102   T   T   T
  0.0727924304960865  0.9018925533036395  0.3251822334614900   F   F   F
  0.7425492398702968  0.2313093825002490  0.4983284754038561   T   T   T
  0.4046858932990643  0.5648725177378805  0.6572709261448455   T   T   T
  0.5657558011652100  0.6610317467383382  0.3472970745831461   F   F   F
  0.2330446902656738  0.9929546137157192  0.5172172097177228   T   T   T
  0.8940268861915768  0.3224552883775441  0.6780015301411285   T   T   T
  0.8403418803460667  0.1680683760692148  0.3362396540223145   F   F   F
  0.5006280651800723  0.5015402424517731  0.5030043685158843   T   T   T
  0.1616345967242424  0.8333832687755323  0.6698358308684962   T   T   T
  0.5657558011652100  0.1568266185306939  0.3472970745831461   F   F   F
```

0.2303310191591664	0.4931109179108396	0.5081322670279343	T	T	T
0.9025331238423073	0.8282875238882919	0.6840171526842901	T	T	T
0.1065177031116420	0.1793101336077285	0.3251822334614900	F	F	F
0.7768948407513958	0.5131118158175267	0.4979447409439833	T	T	T
0.4494608575798271	0.8530970046088893	0.6566904293680145	T	T	T
0.5769975587037308	0.9018925533036395	0.3251822334614900	F	F	F
0.2439354272272909	0.2315611097975864	0.4924926238019418	T	T	T
0.9102194895497998	0.5637217327811656	0.6706870125799957	T	T	T
0.3473785096769433	0.9131343108421603	0.3472970745831461	F	F	F
0.0158577000954202	0.2442414997742089	0.5177688838746987	T	T	T
0.6855038468795808	0.5733680965684473	0.6792245016646110	T	T	T
0.3361367521384224	0.1680683760692148	0.3362396540223145	F	F	F
0.0033319305496261	0.5054994821486778	0.5051306092160451	T	T	T
0.6766410512715554	0.8478717105096863	0.6681387632260795	T	T	T
0.3361367521384295	0.6722735042768520	0.3362396540223145	F	F	F
0.0039459945712938	0.0034449206399607	0.5058905278506660	T	T	T
0.6728458496528704	0.3376225019038003	0.6890644850969084	T	T	T
0.2541842590098113	0.7461778751490158	0.3944775844339503	F	F	F
0.9293433463131867	0.0735446512611372	0.5622607410812681	T	T	T
0.5931871439528108	0.4218364495727688	0.7326924860622437	T	T	T
0.0094723336752622	0.5311979178146160	0.3799386832336822	F	F	F
0.6793280644101294	0.8636877530766407	0.5465855768748524	T	T	T
0.3394561234226149	0.1942900027193413	0.7106379127902328	T	T	T
0.9439217482440156	0.1009536314534927	0.3071906159917361	F	F	F
0.6083089866880114	0.4379161442229675	0.4734541289967611	T	T	T
0.2820120708730500	0.7777359241152615	0.6580721415828314	T	T	T
0.9074566249617817	0.8429681167905230	0.3071906159917361	F	F	F
0.5731838531054667	0.1768348147170957	0.4730340177140030	T	T	T
0.2377419194090969	0.5108082061920968	0.6740050573107570	T	T	T
0.5217255841393538	0.9989379227400192	0.3799386832336822	F	F	F
0.1910934635359919	0.3321078450249222	0.5471375564106956	T	T	T
0.8519015946363352	0.6676543747964545	0.7138273952062060	T	T	T
0.4100411230105863	0.8281303682776340	0.2780017236106858	F	F	F
0.0748935292170952	0.1487374033143720	0.4500847174152147	T	T	T
0.7471038184551456	0.4888996351920167	0.6148250260234529	T	T	T
0.3978860819165106	0.0618058007524454	0.3019131806672561	F	F	F
0.0625587909811741	0.3994916012656501	0.4715558322448228	T	T	T
0.7268998228545924	0.7317523037219976	0.6378001474556400	T	T	T
0.0083537854409172	0.7340228340549402	0.3705661273773728	F	F	F
0.6712588917312609	0.0640443462519714	0.5393411874373445	T	T	T
0.7367620124481107	0.2351831206849297	0.3652886920528999	F	F	F

0.3961900794437526	0.5716573977341588	0.5358113579650542	T	T	T
0.0708164369659432	0.9086410878387484	0.7072119548789332	T	T	T
0.6723299752512091	0.6105241744987708	0.3019131806672561	F	F	F
0.3402256118861722	0.9457290728094764	0.4722381896633815	T	T	T
0.0105202756174768	0.2772611823229675	0.6383525026461777	T	T	T
0.7340793050292973	0.0000564709743571	0.3705661273773728	F	F	F
0.3979509034964979	0.3376548398400999	0.5398850481021332	T	T	T
0.0720322766424246	0.6728602210374091	0.7043748367874915	T	T	T
0.4919936161392044	0.7542259974054701	0.3944775844339503	F	F	F
0.1491611118453568	0.0786520096250295	0.5618365372649828	T	T	T
0.8342152940637999	0.4141410503644049	0.7334541192695255	T	T	T
0.5068313646520934	0.2716482439671637	0.3652886920528999	F	F	F
0.1805315322858237	0.6093906850260248	0.5383358097521227	T	T	T
0.8413378081575922	0.9345350337897737	0.7070578882098069	T	T	T
0.1654421396247585	0.0644885081712587	0.3071906159917361	F	F	F
0.8329495123954804	0.3988393697986977	0.4737085481191511	T	T	T
0.5018277617242883	0.7317324250665189	0.6510788629606753	T	T	T
0.9466044556628361	0.3360802811640724	0.3019131806672561	F	F	F
0.6071298488329843	0.6674932873831874	0.4724375896237019	T	T	T
0.2734873540340686	0.0008859912112453	0.6406598063223978	T	T	T
0.6628011706015897	0.8133490907390950	0.2925406248109539	F	F	F
0.3285722433035433	0.1447406758352429	0.4610843347099443	T	T	T
0.9972163486298431	0.4765332299712851	0.6259637986250680	T	T	T
0.2622323812662657	0.5164166402760770	0.3944775844339503	F	F	F
0.9332715268828188	0.8582234758115713	0.5619161900799012	T	T	T
0.5849515015105737	0.1760299181198327	0.7342635654908055	T	T	T
0.4772123386006655	0.4866846722759277	0.3799386832336822	F	F	F
0.1456424016250452	0.8190931214244587	0.5480587747645645	T	T	T
0.8204504738864007	0.1557252393407261	0.7134768564853020	T	T	T
0.4180892452670406	0.5983691334046952	0.2780017236106858	F	F	F
0.0780483830698038	0.9327006025190614	0.4502530798406537	T	T	T
0.7460009978048637	0.2604097616455022	0.6151877851947916	T	T	T
0.2743874223603413	0.2743309513859842	0.3705661273773728	F	F	F
0.9442955523113458	0.6104975336964832	0.5402025375589125	T	T	T
0.6053632569115425	0.9374269976322844	0.7043013116122279	T	T	T
0.1802798881376475	0.5903210111482409	0.2780017236106858	F	F	F
0.8598837388502033	0.9297940289809760	0.4495251073271653	T	T	T
0.5213485878727087	0.2627199459412165	0.6133202836024254	T	T	T
0.1505479201374982	0.3456090858136918	0.2925406248109539	F	F	F
0.8211868179696818	0.6799101877789665	0.4603509209193510	T	T	T
0.4866350963123519	0.0155795983841390	0.6250886296220661	T	T	T

0.1950611656761865	0.8578623362777833	0.2925406248109539	F	F	F
0.8652063726123850	0.1868470951527732	0.4603014684761499	T	T	T
0.5211773100973879	0.5173735539974247	0.6304518049700721	T	T	T
0.7732271357303446	0.5015788917631880	0.3652886920528999	F	F	F
0.4367409426129548	0.8326498968546051	0.5350246282591797	T	T	T
0.0955908591918391	0.1611203373769022	0.7103292411682827	T	T	T